Biophysical Journal
Article

Biophysical Society

The Influence of Ionic Environment and Histone Tails on Columnar Order of Nucleosome Core Particles

Nikolay V. Berezhnoy,[1] Ying Liu,[1] Abdollah Allahverdi,[1] Renliang Yang,[1] Chun-Jen Su,[2] Chuan-Fa Liu,[1] Nikolay Korolev,[1] and Lars Nordenskiöld[1,*]

[1]School of Biological Sciences, Nanyang Technological University, Singapore, Singapore; and [2]National Synchrotron Radiation Research Center, Hsinchu, Taiwan

ABSTRACT The nucleosome core particle (NCP) is the basic building block of chromatin. Nucleosome-nucleosome interactions are instrumental in chromatin compaction, and understanding NCP self-assembly is important for understanding chromatin structure and dynamics. Recombinant NCPs aggregated by multivalent cations form various ordered phases that can be studied by x-ray diffraction (small-angle x-ray scattering). In this work, the effects on the supramolecular structure of aggregated NCPs due to lysine histone H4 tail acetylations, histone H2A mutations (neutralizing the acidic patch of the histone octamer), and the removal of histone tails were investigated. The formation of ordered mainly hexagonal columnar NCP phases is in agreement with earlier studies; however, the highly homogeneous recombinant NCP systems used in this work display a more compact packing. The long-range order of the NCP columnar phase was found to be abolished or reduced by acetylation of the H4 tails, acidic patch neutralization, and removal of the H3 and H2B tails. Loss of nucleosome stacking upon removal of the H3 tails in combination with other tails was observed. In the absence of the H2A tails, the formation of an unknown highly ordered phase was observed.

INTRODUCTION

In most species of eukaryotes, genomic DNA is packed by nuclear proteins, forming chromatin. Chromatin consists of regular linear arrays of DNA-histone complexes, the nucleosomes. A central part of the nucleosome is the nucleosome core particle (NCP), which is formed by the wrapping of 145–147 bp DNA as a 1.70–1.75-turn superhelix around an octamer of four core histone proteins, two H2A/H2B dimers, and an $(H3/H4)_2$ tetramer (1,2). The NCPs are connected by linker DNA of variable length (10–80 bp), forming a beads-on-a-string chromatin fiber that is further folded into various dynamic secondary and tertiary structures that are still not fully understood. In higher organisms, an additional protein, the linker histone H1, is also regularly present and contributes to chromatin folding, but cells are remarkably tolerant to H1 depletion (3) and it has been shown that fibers with short nucleosome repeat lengths can fold to their natural degree of compaction even in the absence of the H1 histone (4).

NCPs show aggregation behavior similar to that of chromatin fibers, and this phase separation is sensitive to the ionic conditions, with the presence of multivalent cations with charge $\geq +2$ provoking self-association and aggregation (5–14). This sensitivity is due to the polyelectrolyte nature of the NCP, which is a polycation-polyanion complex between the histone octamer (HO) and the DNA (15). Nucleosomal DNA carries a large negative charge (-290e to -294e), which is only partially neutralized by the histones (the total net charge of the HO is $+148$e). The charge of the eight core histones is unevenly distributed between the octamer globular domain ($+60$e) and the eight flexible, unstructured N-termini (the histone tails) (1,16), each of which carries a charge of $+9$e to $+14$e due to a varying number of positively charged lysine and arginine residues. Consequently, the NCP, which has a significant net negative charge (~ -148e), can be visualized as a central particle (-236e) to which the positive flexible tails are attached (15,17). The tails can interact with the DNA of their own NCP, with the linker DNA, and with the other NCPs and proteins present in chromatin. They can also perform important roles in chromatin folding (4,18) and are essential for primary nucleosome-nucleosome interactions (19). Folding and aggregation of chromatin are

Submitted September 28, 2015, and accepted for publication March 7, 2016.

*Correspondence: larsnor@ntu.edu.sg

Nikolay V. Berezhnoy and Ying Liu contributed equally to this work.

Editor: Lois Pollack.

http://dx.doi.org/10.1016/j.bpj.2016.03.016

facilitated and regulated by tail bridging between adjacent NCPs (8,11,20).

Amino acids in the histone tails are subject to numerous posttranslational modifications, with charge quenching acetylations of the ε-amino groups of the lysines being the most frequent and dynamic. Acetylated chromatin is more easily digested by nucleases (21,22) and shows higher solubility in monovalent salt (NaCl and KCl) and in the presence of millimolar concentrations of Mg^{2+} (22–24). The histone tails also play important roles in transcription, replication, repair, and recombination, both as direct modulators of chromatin folding and as a recognition platform for regulatory proteins (25,26). These functions of the tails are regulated through histone modifications, and the presence of tail acetylations typically correlates with transcriptionally active chromatin (27–30).

The cation-induced aggregation of NCPs is similar to the behavior exhibited by other polyelectrolyte systems such as DNA (15,31); however, DNA condensation normally can only be induced by cations with a charge of +3 or higher (32), whereas NCP and chromatin systems can be condensed by divalent cations such as Mg^{2+} and Ca^{2+} (15). NCP-NCP attraction is mediated by the histone tails and is observed in solutions of monovalent salt (8,11) as well as in the presence of Mg^{2+}, whereas under similar conditions, DNA, as well as NCPs and nucleosome arrays lacking the tails, do not show aggregation (4,11) (and references cited in (4)). The close NCP-NCP contact between the flat surfaces of the HO core on both sides of the cylindrical wedge-shaped NCP, called nucleosome stacking, is a common structural feature of the condensed state of chromatin. This stacking has been observed in NCP crystals (1,2,33–35), in NCP liquid crystalline phases (9,10,13,36,37), in the crystal of the tetranucleosome (38), in folded nucleosome arrays (39–41), and in cryo-electron microscopy (cryo-EM) images of frozen isolated native chromatin (42,43).

Various aggregates of NCPs phase-separated in the presence of multivalent cations (or a high concentration of monovalent salt and osmotic pressure) have been systematically characterized by Bertin et al. (13) and Livolant et al. (44) (and references cited therein). These phases include isotropic NCPs similar to the solution-state, NCP columnar phase with no long-range order between columns, as well as the lamello-columnar and highly ordered columnar hexagonal phases (44) (schematically shown in Fig. 1). The phenomenon of supramolecular ordering in NCP aggregates is determined by a complex combination of variables in the mixture and by intrinsic NCP properties. The former include NCP concentration, buffer conditions, cation type, concentration, and osmotic pressure. It was previously shown that the cation-induced formation of condensed NCP phases follows a polyelectrolyte behavior similar to DNA condensation (5). Aggregation of NCPs is dependent on the charge and nature of the cations present in solution (5–7,13), and the histone tails mediate NCP-NCP contacts in a salt-dependent manner (7,8,11,12,14). However, despite all of these observations, knowledge about the molecular structure and thermodynamics of the NCP-NCP contacts, and the precise roles of the tails and tail modifications in the modulation of NCP-NCP interactions and the formation of ordered phases is still limited. Even less is known about the contribution of

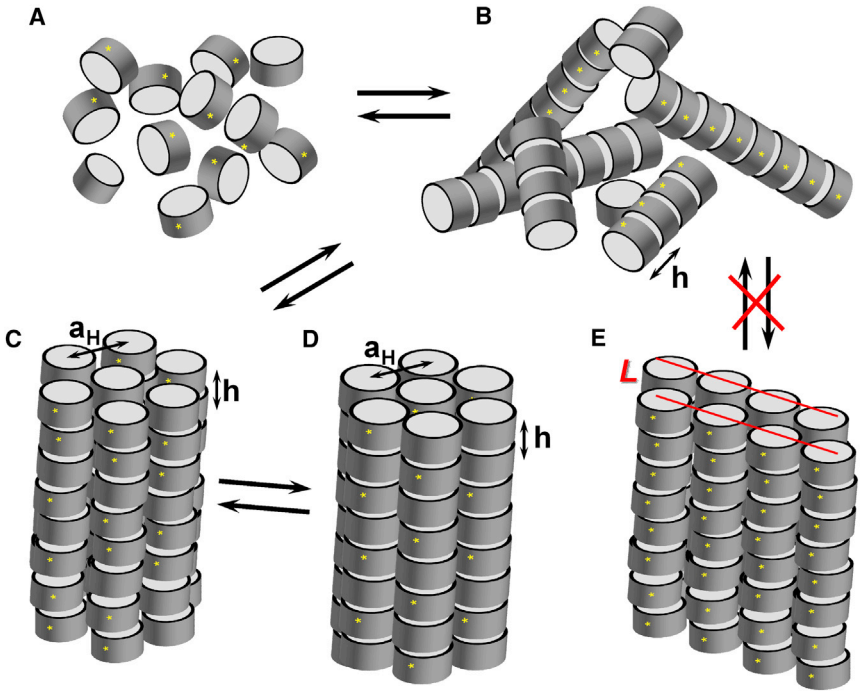

FIGURE 1 (*A–E*) Schematic presentation of the phases formed by NCPs: (*A*) isotropic NCP phase, (*B*) columnar NCP phase, (*C*) 2D columnar hexagonal phase, and (*D*) 3D orthorhombic quasi-hexagonal phase. The distance between stacked NCPs is marked as *h*, the intercolumnar distance is a_H, and *stars* indicate the direction of the dyad axis. (*E*) A single bilayer of the lamello-columnar NCP phase observed by Mangenot et al. (9,10) and Livolant et al. (44) in systems where NCP condensation was caused by osmotic stress and addition of monovalent cations. *Lines* indicate NCP layers in the bilayer. Bilayers in turn formed higher-order structures, with the bilayer-bilayer distance dependent on conditions. To see this figure in color, go online.

intrinsic NCP features, such as the cylindrical wedge shape, inhomogeneous surface charge distribution, dyadic symmetry, and chirality (45–47). Most of the earlier studies used either cell-extracted NCPs or NCPs reconstituted using HOs from chicken blood. These NCPs have intrinsic features with a certain degree of heterogeneity in DNA length, and unknown degrees and positions of histone posttranslational modifications. One can vary the NCP tail and surface charge distribution in a controlled way using recombinant NCPs to address several aspects of nucleosome interactions, in particular modification effects and the roles of histone tails. The synchrotron x-ray diffraction method (using small-angle x-ray scattering (SAXS)) is well suited to address the influence of NCP charge distribution through the detection and characterization of order in the NCP phases (9,10,44–48). The effects of dyadic symmetry and NCP chirality on the order in NCP phases, however, can only be addressed by cryo-EM and optical microscopy methods.

Large quantities of homogeneous NCPs with well-defined DNA sequences can be obtained using recombinant histones (49). Such well-defined systems allow one to determine the contributions of individual tails and specific alterations within them to the association behavior of mononucleosomes. As noted above, much of the previously published data on NCP systems was obtained from cell-extracted chromatin or in solutions of NCPs obtained by nuclease treatment of the chromatin (4,6,9,10,13,50) (and references cited therein). A growing number of studies are using well-defined chromatin and NCPs prepared by recombinant methods (12,14,40,51–58). However, a limited amount of data are available for systems with modifications of the individual histones, such as mutants lacking tails, containing only the globular part of the histone molecule (12), or with selected tail lysines replaced by glutamine (K→Q mutation), mimicking acetylation (40,51–56,59). Published results indicate that acetylation or the absence of tails stabilizes NCPs or arrays in the solution state against self-association and promotes the unfolding of compact nucleosome arrays (12,51–53,58,60). The H4 tail (12,52,61,62) and specifically H4-K16 (51,55,58) have been found to be critical for intramolecular folding of individual nucleosome arrays. Of note, one of the H4 K16-R23 regions (of the two H4 tails) is involved in NCP stacking, since it is located between the two NCPs in practically all reported NCP crystal structures, interacting with the acidic patch located on the globular domain of the H2A histone of the neighboring NCP (1,63).

In this work, we characterized the x-ray diffraction spectra of various precipitated NCP samples and their Bragg peak patterns (using the synchrotron SAXS beamline) to investigate the supramolecular structure in NCP aggregates, complemented by a SAXS dilute-solution investigation for selected samples. We studied the effects caused by H4 tail acetylations or deletions of tails on the supramolecular structure of NCPs aggregated by Mg^{2+} and cobalt(III)hexammine ($CoHex^{3+}$) cations. Wild-type (WT) and mutant NCPs were reconstituted from recombinant *Xenopus laevis* histones with a 145 bp DNA fragment of the 601 nucleosome positioning sequence (64). Specifically, NCPs containing H4 histones with lysines acetylated at the K16 position (H4-K16Ac) and at the K5, K8, K12, and K16 positions (H4-QuadAc) were investigated. To compare the effects of acetylations with K→Q mutations (both quenching the lysine charge), NCPs containing H4 tails mutated at the same K5, K8, K12, and K16 positions (H4-K16Q and H4-QuadQ) were studied. The effect of H2A histone acidic patch neutralization was investigated. Additionally, the effects of deletion of individual tails and combinations thereof were investigated. In a recent work using well-defined recombinant NCPs, we investigated the effects of H4 tail acetylation and deletion of tails on cation-induced NCP aggregation (20), and the work presented here complements that study.

MATERIALS AND METHODS

A detailed description of the materials and methods applied in this work is given in Supporting Materials and Methods in the Supporting Material. Below, a brief account of the applied techniques is presented.

Preparation of NCPs

Recombinant WT, mutated, and truncated *X. laevis* core histone proteins H2A, H2B, H3, and H4 were expressed in the *Escherichia coli* [BL21 (DE3) pLysS] strain and purified by gel-filtration and cation-exchange chromatography. H4 histones containing acetylated lysine, H4-K16Ac, and H4-QuadAc (H4 histone with lysine residues acetylated at positions 5, 8, 12, and 16) were synthesized by natural chemical ligation and purified as described previously (58).

The HOs were refolded by dialysis from a mixture of WT or modified core histones H2A, H2B, H3, and H4, and purified by gel-filtration chromatography. The purity and completeness of the HO refolding was checked by 18% SDS-PAGE.

The 145 bp DNA of the 601 Widom nucleosome positioning sequence (64) was used in this work to reconstitute NCPs. In a few measurements, NCPs reconstituted with the 147 bp palindromic human α-satellite DNA fragment (1,2) were also used. The 145 bp 601 DNA construct in the pUC19 plasmid was amplified using the *E. coli* HB101 strain, extracted by the alkaline lysis method, released by EcoRV, and separated by PEG 6000.

The NCPs were reconstituted from DNA and HO by a stepwise dialysis in a high- to low-salt buffer (49,65,66). The best yield was obtained for the WT NCPs; reconstitution of the NCPs with mutated and deleted tails was less efficient, but still was notably better than that described by Bertin et al. (12,14) for tailless NCP constructs. The quality of the reconstitution was assayed by 5% PAGE (see Fig. S3 *C*), yielding an estimated presence of <5% of free DNA. After NCP precipitation from solution by multivalent cations for the x-ray diffraction measurements, any free DNA will remain in the supernatant and this stage acts as a further purification.

Sample preparation, data collection, and analysis

We investigated the structures of cation-induced NCP aggregates using SAXS, where ordered phases can be identified from the way they diffract x-rays. Table S1 contains a summary of more than 200 analyzed samples.

Along with WT-NCPs assembled with HO consisting of recombinant, fully charged histones, we reconstituted four variants of the NCP using various H4 histones with single- or tetra-acetylated or mutated lysine residues in the histone tail: H4-K16Ac, H4-QuadAc, H4-K16Q, and H4-QuadQ. Additionally, one HO was prepared with three charge-neutralizing mutations in the acidic patch of the H2A histone (the mutations were D90S+E91T+E92T, abbreviated as H2A-STT). The other NCP samples contained various combinations of tailless histones. NCP aggregation was induced by addition of divalent Mg^{2+} or trivalent $CoHex^{3+}$ cations. Aggregation of a few samples of WT-NCP was also induced by the polyamines spermidine^{3+} (Spd^{3+}) and spermine^{4+} (Spm^{4+}). The final concentration of the NCP was 8 mg/mL. For comparison and reference purposes, solution SAXS spectra for WT-NCP solutions in a concentration range of 1.25–17 mg/mL NCP and two concentrations of KCl (10 and 100 mM) were obtained. Furthermore, solution spectra of the H4K16Q, H4-QuadQ, gH2A, and gH2BgH2B samples were collected for two concentrations of KCl.

High-energy synchrotron radiated x-rays were used to compensate for the weak scattering intensity of the biological samples. The samples were prepared as described in Supporting Materials and Methods. Measurements were made at the beamline 23A SWAXS end-station at the National Synchrotron Radiation Research Center (Hsinchu, Taiwan) (67). Some samples were repeatedly measured at intervals of several months with no apparent changes in the spectral characteristics (data not shown).

The phases of the NCP aggregates were identified from the periodicity of the Bragg peaks as a function of the scattering vector q. NCP stacking and hexagonally ordered columns generate sets of peaks with a periodicity of 1:2:3:4 and 1:$\sqrt{3}$:$\sqrt{4}$:$\sqrt{7}$:$\sqrt{9}$, respectively (9,44,68). The NCP stacking distance h and the intercolumnar distance a_H in columnar hexagonal phases (Fig. 1, *C* and *D*) were calculated from the position of the first peaks, q_{1h} and q_1, using the equations $h = 2\pi/q_{1h}$, and $a_H = 2/\sqrt{3}\cdot 2\pi/q_1$. Fig. 2 displays an example of an x-ray diffraction spectrum with annotated peaks.

RESULTS AND DISCUSSION

We used SAXS to study the effects of lysine acetylations in the H4 histone tails, neutralization of the acidic patch on the H2A globular domain, and removal of histone tails in the recombinant NCP aggregated by Mg^{2+} and $CoHex^{3+}$ cations (Table S1). In addition, H4-K16Q, H2A-STT, gH2A, and gH2AgH2B samples in solution at two concentrations of monovalent KCl were investigated.

Solution SAXS spectra

The diffraction spectrum intensity $I(q)$ originates from x-rays scattered by the atoms of individual NCPs (by the form factor, $P(q)$) and by the structures formed by interacting NCPs (by the structure factor, $S(q)$), hence $I(q) \sim P(q) \times S(q)$). Fig. 2 shows spectra of the WT-NCP recorded in the presence of five cations, namely, K^+, Mg^{2+}, $CoHex^{3+}$, and the polyamines Spd^{3+} and Spm^{4+}. It is well established that at low concentrations of monovalent cations (K^+ or Na^+), the interaction between nucleosomes is weak and repulsive (7,48). Therefore, the SAXS spectrum obtained from the solution of homogeneous and isotropic NCPs is primarily defined by the form factor $P(q)$ of the NCPs (*top magenta curve* in Fig. 2). For the WT-NCP, we recorded SAXS spectra of NCP solutions with 10 and 100 mM KCl in a range of NCP concentrations from 1.25 to 17 mg/mL (see Fig. S1). Our results agree with the solution SAXS data reported by others

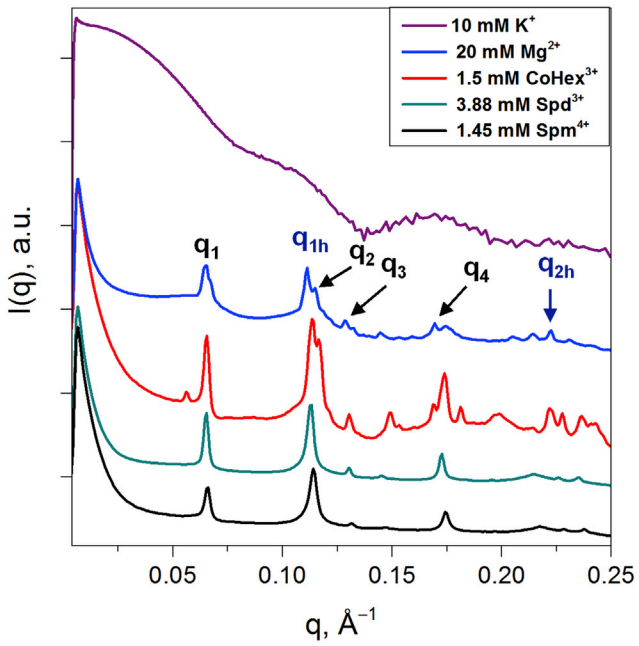

FIGURE 2 SAXS spectra of the solution and most-ordered phases of WT-NCP with cations (the nature and concentration of the ions are indicated in the graph). The solution SAXS spectrum of WT-NCP at 1.25 mg/mL in 10 mM KCl (*top spectrum*) largely overlaps with the profile calculated from the atomic coordinates of the NCP crystal structure 1KX5 (2) (see Fig. S2). In the presence of multivalent cations (*second to last spectra from the top*), NCPs precipitated from solution form ordered columnar hexagonal structures. On the spectrum in the presence of 20 mM Mg^{2+}, the peak characteristics of the 3D orthorhombic order (q_1, q_2, q_3, and q_4) due to NCP-NCP stacking within the columns (q_{1h} and q_{2h}) are indicated. To see this figure in color, go online.

(7,14,48). At low NCP concentrations (C_{NCP} = 1.25 and 2.5 mg/mL) in 10 mM KCl, the experimental SAXS profiles show an almost perfect overlap with the simulated spectrum calculated from the atomic structure of the NCP obtained from molecular-dynamics simulations (69), which compared with the NCP structure in the crystal (2) exhibits collapse of the histone tails on the globular part of the NCP. According to physicochemical principles (70), oligocationic tails should be bound to polyanionic DNA under low-salt conditions, and this most realistic NCP structure shows the best agreement with the measured SAXS spectrum. NCP structures with the tails extended outside of the globular part or with the tails removed showed worse agreement with experimental data. We used two programs to simulate SAXS spectra from atomic coordinates, CRYSOL (71) and FoXS (72) (Fig. S2), which produced very similar results.

We used the experimental form factor of the WT-NCP obtained at C_{NCP} = 1.25 mg/mL in 10 mM KCl to estimate the structure factors of the WT-NCP in solution. The scattering profiles together with calculated structure factors (Fig. S1, *C* and *D*) allow a better assessment of the NCP ordering when broad maxima in scattering vector ranges of 0.09–0.10 and 0.16–0.17 $Å^{-1}$ of the $P(q)$ profile contribute significantly and overlap with peaks from weak NCP-NCP interactions.

Samples of WT-NCPs show little interaction in both 10 and 100 mM KCl. At 10 mM KCl, an increase in the NCP concentration results in a progressive drop of the intensity of the $S(q)$ profile at low q-values (Fig. S1 *C*), indicating repulsive NCP-NCP interactions. In contrast, at 100 mM KCl, weak maxima observed at 0.012–0.016 $Å^{-1}$ (Fig. S1 *D*) are likely to indicate the weak attractive NCP-NCP interactions as reported by others for NCP solutions with increased concentrations of NaCl and NCP (7,11,48).

The scattering from solutions of selected mutated and tailless NCPs was recorded to assess the form factor that could indicate the change in shape of the particles caused by modifications. Selected SAXS profiles recorded for the WT-NCP, H4-K16Q, and H2A-STT NCPs are compared in Fig. S3 *A*. Fig. S3 *B* shows spectra in solutions of the WT-NCP, gH2A, and gH2AgH2B NCPs. Figs. S4 and S5 present all solution SAXS spectra collected for the selected mutated and tailless NCPs. H4-K16Q, and H2A-STT samples produced scattering spectra with features almost identical to the WT-NCPs (Fig. S3 *A*). The results in Fig. S3 *A* demonstrate (together with the corresponding gels in Fig. S3 *C* and other assays, data not shown) that modifications/mutations have only minor effect on the particle shape and size and that our systems are homogeneous, which is known from previous studies with these constructs. The tailless particles on the other hand, produced featureless spectra, distinct from the WT-NCP (Fig. S3 *B*). These spectra are in agreement with the spectra reported by Livolant and colleagues (14). The absence of the minima as the most pronounced effect of tail deletion was suggested to originate from a change in DNA wrapping around the octamer core and may also indicate that DNA wrapping is more dynamic and flexible.

Cation-induced condensed phases of WT-NCP

The formation of ordered phases by WT-NCP (i.e., for histones without any modifications or tail deletions) in a range of concentrations of Mg^{2+}, $CoHex^{3+}$, Spd^{3+}, and Spm^{4+} was investigated (Figs. 2, 3, S6, and S7; Tables S1 and S2). Upon addition of multivalent cations, the highly homogeneous recombinant NCPs instantaneously aggregate, and precipitate upon gentle centrifugation (see Supporting Materials and Methods). In a certain cation concentration range, highly ordered phases were identified from SAXS spectra (Fig. 2). The spectral features are reproducible without significant changes for periods from immediate measurements within days of preparation up to several months (data not shown).

Columnar hexagonal phases are formed in solutions of WT-NCP in the presence of millimolar concentrations of Mg^{2+}, $CoHex^{3+}$, Spd^{3+} and Spm^{4+} as indicated by a clear appearance of the characteristic hexagonal order peaks, q_1, q_2, q_3, and q_4 at ~0.065, 0.113, 0.13, and 0.172 $Å^{-1}$, with the expected ratio of $1:\sqrt{3}:\sqrt{4}:\sqrt{7}$ (Fig. 2). The set of peaks

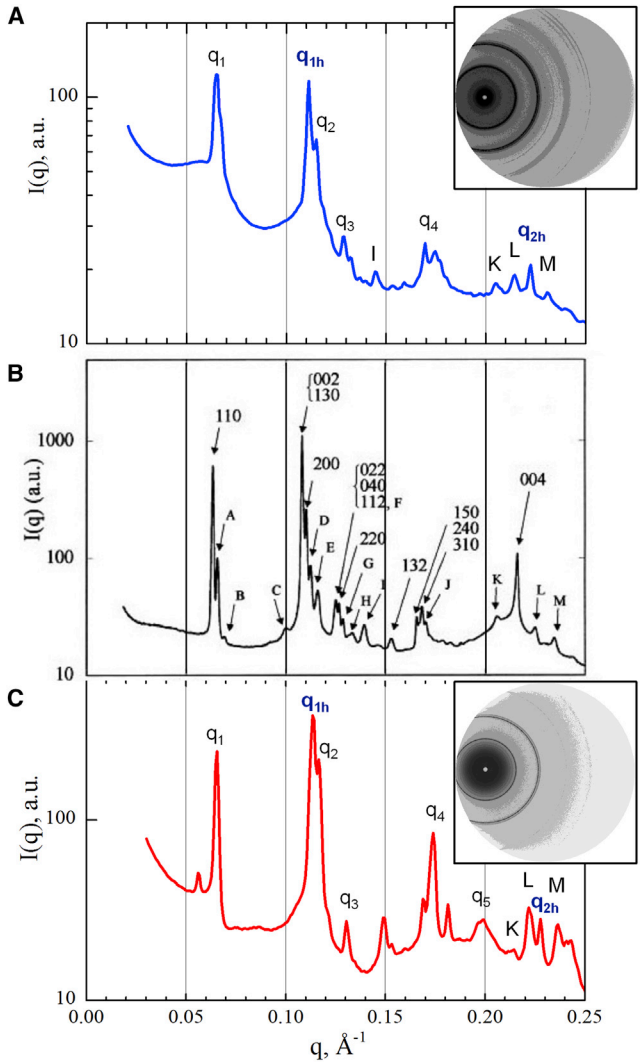

FIGURE 3 (*A* and *C*) Spectra of highly ordered phases formed by WT-NCP in the presence of 20 mM Mg^{2+} (*A*) and 1.5 mM $CoHex^{3+}$ (*C*). The insets show corresponding SAXS diffraction patterns. (*B*) The spectrum for NCPs obtained from nuclease-digested calf thymus chromatin in 160 mM NaCl under an osmotic pressure of 4.7×10^5 Pa after 4 months of equilibration and after partial orientation in a 10 T magnetic field for 15 days (9) is shown for comparison. In (*B*), peaks are marked according to the periodicity of the orthorhombic lattice (a, b, c) with dimensions (a_H, $\sqrt{3} \times a_H$, ~h). Peaks indicated by letters from A to M are suggested to correspond to a superstructure along the c-axis of a periodicity close to 6c: A (1, 1, 1/3), B (1, 1, 1/2), C (0, 2, 1 + 1/2), D (1, 3, 1/2), E (0, 0, 2 + 1/6), F (0, 0, 2 + 1/3), G (0, 4, 1/2) and (2, 2, 1/2), H (0, 0, 2 + 1/2), I (2, 1, 1 + 1/2), J (3, 1, 1/2), K (3, 3, 1 + 1/2), L (0, 0, 4 + 1/6), M (0, 0, 4 + 1/3). Panel (*B*) is reprinted with permission from the Biophysical Society. To see this figure in color, go online.

with a 1:2 ratio at ~0.11 and 0.22 $Å^{-1}$, assigned respectively as q_{1h} and q_{2h} indicate columnar stacking of the NCPs. The most ordered WT-NCP aggregates were observed at 20 mM Mg^{2+}, 1.5 mM $CoHex^{3+}$, 3.88 mM Spd^{3+}, and 1.45 mM Spm^{4+} (Fig. 2; Table S2). The presence of only $q_{1,2,3}$ and $q_{1h,2h}$ peaks, illustrated by spectra for WT-NCP with Spd^{3+} and Spm^{4+} indicates a two-dimensional (2D) columnar

hexagonal phase. The presence of peaks in addition to the columnar hexagonal phase, illustrated in spectra from the WT-NCP with Mg^{2+} and $CoHex^{3+}$, indicates the formation of a three-dimensional (3D) orthorhombic quasi-hexagonal phase. The additional peaks indicate correlation between columnar and hexagonal orders like in a crystal. This interpretation was developed by Mangenot et al. (9) and Livolant et al. (44), who used the intercolumnar distance a_H and NCP stacking distance h to characterize the hexagonal phase, and *a, b, c* indices for the orthorhombic quasi-hexagonal phase. The orthorhombic quasi-hexagonal phase has a slightly distorted hexagonal order, with peak positions deviating by ~2% from the hexagonal periodicity. In this work, although we distinguish between phases with 2D columnar hexagonal and 3D orthorhombic quasi-hexagonal order, we use the 2D notation for both.

The NCP stacking distances $h = 55$–57 Å and the intercolumnar distances $a_H = 110$–112 Å calculated from the SAXS spectra of the WT-NCP are inversely related to the cation charge, being the shortest for the Spm^{4+} and largest for the Mg^{2+} ions, indicating the relative compactness of the NCP packing (Table S2). Previous computational studies have also shown more condensed internucleosome packing induced by $CoHex^{3+}$ compared with Mg^{2+} (20,57,58). The characteristic distances observed for recombinant WT-NCPs that were precipitated by multivalent cations were generally comparable or less than the values reported for native cell-extracted NCPs condensed by osmotic shock in the presence of NaCl ($h = 57.7$–60 Å and $a_H = 110$–116 Å) (44).

The 3D orthorhombic quasi-hexagonal symmetry in NCP aggregates is not unexpected given the orthorhombic packing obtained for single crystals of NCPs (1,2). In Fig. 3, we compare our spectra of ordered WT-NCP phases condensed by Mg^{2+} and $CoHex^{3+}$ with a spectrum previously obtained for highly ordered NCPs prepared from nuclease-digested calf thymus chromatin, aggregated by osmotic pressure at a high monovalent salt concentration, oriented in a magnetic field for 15 days and measured after 4 months of equilibration (9,44). The comparison allows us to index some of the correlation peaks in our x-ray diffraction spectra. However, our assignment is incomplete and should be considered tentative, and furthermore, our samples were not oriented and thus were more disordered. It is challenging to assign all diffraction peaks from the averaged one-dimensional x-ray diffraction spectrum from a polycrystalline sample. 2D spectra with the phase information from single crystals are needed to unequivocally assign all peaks and determine the structure. However, it is clear that the recombinant WT-NCP samples aggregated by Mg^{2+} or $CoHex^{3+}$ are indicative of a degree of ordering similar to that previously obtained under conditions that favor high order (9,44). This shows that the formation of highly ordered columnar hexagonal phases is a natural characteristic of mononucleosomes that likely corresponds to the equilibrium phase under physiological conditions.

The polyelectrolyte behavior of NCP interactions in a wide range of Mg^{2+} concentrations is noteworthy. A gradual loss of hexagonal order is observed at cation concentrations significantly lower or higher than 20 mM (Fig. S6 *A*). In the range of 8–14 and 24–50 mM Mg^{2+}, an NCP columnar phase with no long-range order is observed. The broad peaks arise from the average intercolumnar distance (q_1 ~0.065 $Å^{-1}$), the average NCP stacking distance within columns, and the columnar form factor from the local arrangement (q_2 and q_{1h} ~0.11 $Å^{-1}$ and q_3 ~0.17 $Å^{-1}$) (44). At 3 and 80 mM Mg^{2+}, an isotropic NCP phase is observed, and the spectra are similar to the form factor obtained from a solution of WT-NCP. At Mg^{2+} concentrations lower than 3 mM or higher than 80 mM, the NCPs remain soluble. In contrast, a stable columnar hexagonal phase is observed in a broad range of $CoHex^{3+}$ concentrations (1.5–30 mM), with an isotropic NCP phase being observed at 1.2 mM $CoHex^{3+}$ (see Fig. S6).

We also obtained x-ray diffraction spectra for a few samples of NCPs reconstituted with a different DNA template, namely, the 147 bp palindromic human α-satellite DNA fragment. The spectra are shown in Fig. S8 and the pattern shows a 2D hexagonal columnar phase, displaying sharp peaks, in addition to some weak additional peaks indicating distortion from the 2D hexagonal arrangement. Consequently, the columnar hexagonal phase was obtained for mononucleosomes extracted from cells that likely contain an unknown amount of posttranslational modifications in the histone tails (Livolant et al. (44)).

Supramolecular structures for NCPs with modified and tailless histones

Spectra representing the most ordered phases for NCPs with various histone modifications obtained in presence of Mg^{2+} or $CoHex^{3+}$ are summarized in Fig. 4. The concentration ranges of Mg^{2+} and $CoHex^{3+}$ investigated for each variant of NCP and the type of the most ordered phase are schematically presented in Fig. 5 (see also Table S2 and Figs. S9–S22). In Fig. 4 the spectra are divided into three groups: 1) NCPs with mutated and acetylated histones (H2A-STT, H4-K16Q, H4-K16Ac, H4-QuadQ, and H4-QuadAc; Fig. 4, *A* and *B*); 2) NCPs with one of the four histone tails truncated (gH2A, gH4, gH2B, and gH3; Fig. 4, *C* and *D*), and 3) NCPs lacking two or more histone tails (gH2AgH2B, gH3gH4, gH2AgH3gH4, gH2AgH2BgH3, and gNCP; Fig. 4, *E* and *F*). Within each graph the spectra are aligned in the order that reflects the change of the charge in the HO relative to the charge of the WT-NCP (numbers are shown between the Mg^{2+} and $CoHex^{3+}$ panels). All modifications, excluding H2A-STT, increase the net negative charge of NCPs. Changes in the NCP charge and charge distribution alone may alter the NCP structure and affect NCP-NCP interactions, which in turn may influence the degree of order within the NCP aggregates in a cation-dependent manner. In addition, acetylation or tail deletion may affect the NCP

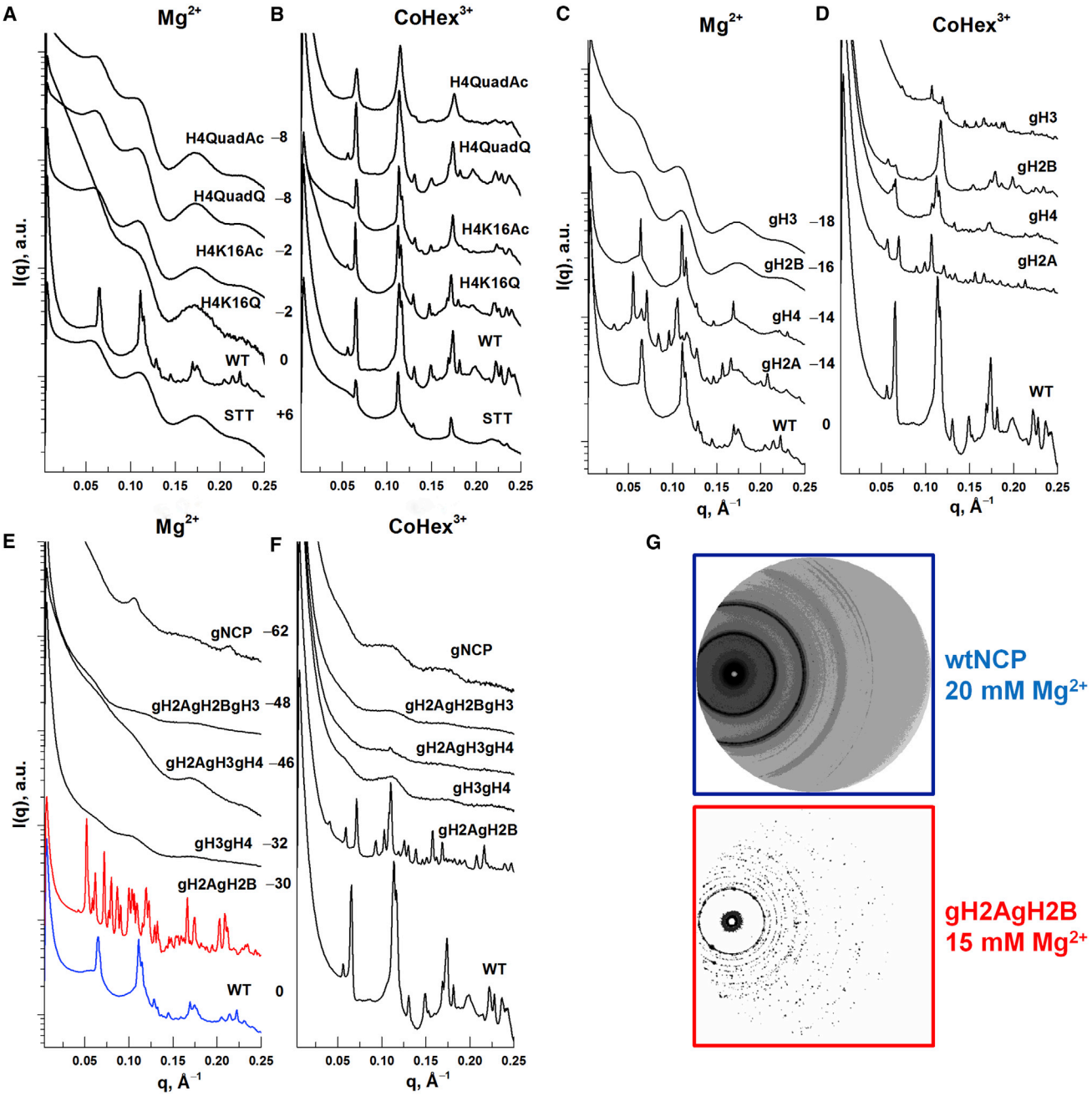

FIGURE 4 (*A–F*) SAXS spectra for NCPs with various histone modifications and with added Mg^{2+} (*A*, *C*, and *E*) or $CoHex^{3+}$ (*B*, *D*, and *F*). (*A* and *B*) NCPs with octamers containing mutated or H4-acetylated histones. (*C* and *D*) NCPs with HOs lacking tails in one of the four histones (gH2A, gH2B, gH3, and gH4). (*E* and *F*) NCPs with octamers lacking tails in two or more of the four histones. For each NCP modification, the concentrations of Mg^{2+} and $CoHex^{3+}$ were varied and the SAXS spectrum corresponding to the most-organized NCP phase is shown. All spectra are given in Figs. S9–S22. In each panel, the WT-NCP SAXS profile is given for comparison; the change of the net NCP charge relative to the WT-NCP is indicated next to the sample identifiers. (*G*) Two types of NCPs containing tailless histone H2A (gH2A and gH2AgH2B) form highly ordered structures that are different from all other NCP variants. Shown is a comparison of SAXS patterns recorded in the presence of Mg^{2+} for WT-NCP (*top frame*) and gH2AgH2B (*bottom frame*). Corresponding 1D spectra are shown in panel (*E*). To see this figure in color, go online.

structure and NCP-NCP interactions in a cation-independent manner, combining electrostatic and steric contributions.

All of our results are subject to the assumption that we were able to detect the most ordered state in the range of measured concentrations of counterions.

One noticeable feature of the SAXS spectra shown in Fig. 4 is that NCP samples with $CoHex^{3+}$ generally display a columnar hexagonal order, except for the NCPs lacking two or more histone tails. Samples with the corresponding NCPs aggregated by Mg^{2+}, in contrast, display columnar

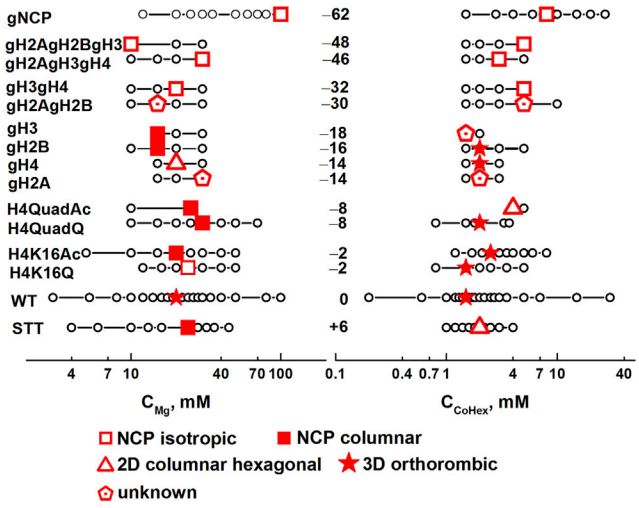

FIGURE 5 NCP samples with different variants of core histones studied in a range of concentrations of Mg^{2+} (*left*) and $CoHex^{3+}$ (*right*) salts. Numbers show the change of the net NCP charge relative to the WT-NCP. Circles show the studied Mg^{2+} or $CoHex^{3+}$ concentrations, and the concentration that resulted in the most-ordered NCP phase for a given sample is indicated by a *symbol*. The corresponding NCP phases are listed below the chart. To see this figure in color, go online.

hexagonal phases, columnar disordered phases, and the isotropic NCP phase.

The H4-K16Q, H4-QuadQ, and H4-K16Ac NCPs show a degree of order and phase behavior rather similar to the WT-NCP in the presence of $CoHex^{3+}$. The H2A-STT NCP, in contrast, shows a columnar hexagonal order only at 2 mM $CoHex^{3+}$ and a disordered columnar phase for $CoHex^{3+}$ concentrations in the 1.2–4 mM $CoHex^{3+}$ range measured. The limited measurements obtained with H4-QuadAc show a columnar hexagonal phase in the presence of $CoHex^{+3}$, and based on the similarity in the effects of K16Q and K16Ac modifications, we assume that the H4-QuadAc modification effect is similar to the H4-QuadQ one. The characteristic NCP stacking and intercolumnar distances in the columnar hexagonal phases of NCPs with modified histones are in the range of h = 54.6–55.9 Å and a_H = 109.9–111.8 Å. Interestingly, no apparent dependence on the nature (acetylation versus K→Q mutation) and number (single H4-K16 or tetra H4-K5, K8, K12, or K16 change) of lysine modifications was observed.

With the more biologically relevant Mg^{2+}, the columnar hexagonal phase was not achieved for all five mutated NCPs. The absence of hexagonal order appears to be cation dependent, because well-ordered columnar hexagonal phases were observed for the NCP variants with mutated or modified histones in the presence of $CoHex^{+3}$ (Fig. 4 *B*). The NCP columnar phase was observed for all but H4-K16Q. The latter showed an isotropic NCP phase. The modifications in the H4 histone tails, as well as the STT mutation in the H2A histone, led to significantly reduced order compared with the WT-NCP in the presence of Mg^{2+} (Fig. 4 *A*). The investigated modifications in the presence of Mg^{2+} seemed to prevent the ordering of NCP columns.

We observed two specific effects of the mutations: 1) the H2A acidic patch neutralization greatly reduced the $CoHex^{3+}$ range for columnar hexagonal phase formation, and 2) H4-K16Q prevented NCP stacking in the presence of Mg^{2+}. The neutralization of three negative charges on the NCP stacking interface had a destabilizing effect on the columnar hexagonal phase in comparison with neutralization of one or four positive charges on H4 tail. The observed difference may be due to the nature or the location of the neutralized charges and is analogous to a similar disruption of the NCP-NCP contacts in folding of nucleosome arrays reported for the H2A.Bbd variant of the histone H2A with charge-quenching alteration of the acidic patch (73).

The removal of histone tails from one core histone shows that not all tails are equal (Fig. 4, *C* and *D*). The absence of H2B and H3 tails led to formation of the columnar NCP phase in the presence of Mg^{2+} and columnar hexagonal phases in the presence of $CoHex^{3+}$ in a cation-dependent manner. For both Mg^{2+} and $CoHex^{3+}$, removal of the H4 tails did not affect the formation of columnar hexagonal phases, which is similar to the behavior exhibited by the WT-NCP. Surprisingly, in the presence of either of the two cations (Mg^{2+} and $CoHex^{3+}$), the NCP with truncation of N-terminal as well as C-terminal tails in the H2A histones produced x-ray diffraction spectra with a large number of peaks that were not previously observed for NCPs here or in the literature. The gH3 samples displayed spectra with peak patterns similar to those observed for gH2A with 2 mM $CoHex^{3+}$. A possible interpretation of these spectra is that there is a mixture of more than one phase, including one of hexagonal order. The removal of tails has no effect on phase structure in the case of the histone H4, is cation dependent for the histones H3 and H2B, and leads to structural changes for the H2A histone.

NCP systems lacking tails in two (gH3gH4), three (gH2AgH3gH4, gH2AgH2BgH3), or all four histones (gNCP) did not form columnar hexagonal phases with Mg^{2+} and $CoHex^{3+}$ (Fig. 4, *E* and *F*). The gNCP samples displayed peaks characteristic of NCP stacking at 80 and 100 mM Mg^{2+}, and the isotropic NCP phase was observed in the 12–60 mM Mg^{2+} range. The NCP samples gH3gH4, gH2AgH2BgH3, and gH2AgH3gH4 resembled gNCP in the 10–30 mM Mg^{2+} range, forming an isotropic NCP phase. All NCP samples lacking more than one tail mentioned above formed isotropic NCP phases in the range of 1.5–5 mM $CoHex^{3+}$ (gNCPs were measured in a broader range of 1.5–27 mM $CoHex^{3+}$).

In the presence of Mg^{2+}, the gH2AgH2B samples display unusual spectra with sharp peaks, indicating long-range order such as that found in a crystal (see the spectrum highlighted by *red* in Fig. 4 *E*). These are similar to the spectra of

the gH2A sample, and the diffraction pattern reveals a crystal-like organization (Fig. 4 *G*, bottom spectrum in the *red frame* compared with the spectrum from the WT-NCP). It seems likely that these spectra are due to the formation of at least two phases, one of which could be the commonly observed columnar hexagonal structure (the expected hexagonal peaks can be tentatively assigned). It appears that the removal of the H2A and H2B tails resulted in the formation of highly ordered phases of yet unknown structure. The spectra of gH2AgH2B at 1.5 or 5 mM $CoHex^{3+}$ are very similar to the gH2A spectra at 2 mM $CoHex^{3+}$. The same set of peaks of higher intensity for the former is shifted to a higher q range, indicating tighter packing. Thus, we suggest that the same phase of unknown structure and long-range order is formed by NCPs lacking H2A tails and by NCPs lacking H2A and H2B tails in the presence of Mg^{2+} and $CoHex^{3+}$. The formation of the columnar hexagonal phase by gH2AgH2B NCPs was also observed in the presence of $CoHex^{3+}$. Currently, it is not possible to suggest what sort of structure is formed, and additional experiments are needed to gain insight into this effect.

In general, it was observed that the ordering of the NCP aggregates decreased as the number of tailless histones increased (with the notable exceptions of the gH2A and gH2AgH2B systems). The order decreased in both the NCP stacking and the hexagonal columnar association.

Two broad diffraction peaks with a 1:2 positional ratio observed in the spectra of gNCPs at 80 and 100 mM Mg^{2+} (Figs. 4 *E* and S22) indicate a possible NCP stacking of short-range order with a mean distance $h = 59.4$ Å (Table S2). This distance is significantly larger than that observed for the other NCP variants, suggesting very loosely stacked NCP aggregates. It may be noted that the electrophoretic mobility of the gNCP is slower than that of the WT and the mutated/acetylated NCPs (20), suggesting that the gNCPs may have an extended size, probably due to detachment of the entry/exit parts of the DNA from the histone core. A similar DNA detachment effect may apply to the gH2AgH3gH4 sample, where a weak peak corresponding to $h = 57.1$ Å was observed at 3 mM $CoHex^{3+}$ (Fig. 4 *F*; Table S2). The absence of columnar ordering in these spectra may suggest a smectic NCP organization with layers of NCP that lack proper stacking and are laterally disordered due to the extended DNA.

Studies of NCPs concentrated by variation of the osmotic pressure in the presence of monovalent salt have identified the formation of bilayers of NCPs stacked in columns that are also visible in EM images and show a scattering peak q_{1L} at low q corresponding to a distance of ~350 Å (9,10,44). However, in our study, as well as in other studies of ordered phases in the presence of multivalent cations (13,74), the bilayer phase was never observed. Such a loose bilayer arrangement was seen in NCP systems with monovalent salt and under osmotic pressure (44) (and references therein). In general, multication-induced condensation of DNA (31,75) and nucleosome arrays (76) proceeds as a cooperative process, an all-or-nothing transition. It is reasonable to expect that NCP aggregation would follow the same process. Therefore, under the conditions applied here, one would expect the existence of either NCPs in solution or fully condensed phases of NCPs without bilayer intermediates.

Estimation of the size of the columnar hexagonal NCP domains

A lower boundary of the linear domain size s of the ordered aggregates can be estimated from the fitted full width at half-maximum (FWHM) of the first diffraction peak, namely, $s = 2\pi/\text{FWHM}$. In the columnar hexagonal NCP phase, the length across the columnar hexagonal domain $s(a_H)$ and the length of the NCP columns $s(h)$ can be estimated using the FWHM of q_1 and q_{1h} peaks, respectively. The domain sizes of columnar hexagonal phases are listed in Table S3. The number of columns and stacked NCPs in the column may be calculated by dividing the domain size $s(a_H)$ and $s(h)$ by a_H and h, respectively. A WT-NCP columnar hexagonal phase made of 20–30 columns, each consisting of 40–50 NCPs as estimated from the SAXS data, agrees with previous observations made using cryo-EM (44). A reduction in domain size in comparison with the WT-NCP was observed for H4-QuadAc and gH2B with $CoHex^{3+}$, whereas the opposite effect was observed for H4-K16Q with $CoHex^{3+}$ and for gH4 with Mg^{2+}. The general observation was a larger number of NCPs stacked in the column compared with the number of arranged columns.

CONCLUSIONS

In solutions with low (<50 mM) monovalent salt, interactions between NCPs are repulsive. The addition of millimolar concentrations of Mg^{2+} or $CoHex^{3+}$ results in phase separation and the formation of NCP aggregates with different arrangements of particles, ranging from the isotropic NCP phase to NCP columnar and columnar hexagonal phases. The major contribution to free energy that drives phase separation comes from the entropic gain of the release of monovalent counterions (15).

The x-ray diffraction method enabled us to quantitatively assess the short- and long-range order in many NCP aggregates, and to identify and distinguish a number of known phases with NCP stacking and columnar arrangement order. These advantages compensate for the limitations of polycrystalline samples of higher disorder, incomplete sampling that assumes detection of the most ordered phases, and the inability to solve the structure with regard to the order of dyad symmetry and NCP chirality in general, and for some of the tailless NCPs in this work in particular.

Our results are in general agreement with earlier x-ray diffraction studies (9,10,44) in which a variety of NCP

phases were observed. Compared with previous studies performed on inhomogeneous nucleosomes extracted from native chromatin (9,10,44), we observed more compact packing and faster equilibration of the highly homogeneous recombinant NCPs. The WT-NCP stacking distances in the range of $h = 55–57$ Å and intercolumnar distances of $a_H = 110–112$ Å are shorter and more uniform than those observed for cell-extracted NCPs.

In the 3–80 mM Mg^{2+} range, the phase behavior of the WT-NCP aggregates is dependent on the cation concentration. With increasing Mg^{2+} concentration, the order changes from isotropic NCP to columnar disordered and finally columnar hexagonal. A further increase in Mg^{2+} concentration leads to the same set of phases in reverse order. Our observations suggest a model of columnar hexagonal phase formation in which column formation by NCP stacking is followed by intercolumnar interactions. For $CoHex^{3+}$, the isotropic NCP to 3D to 2D columnar hexagonal phase transition in the narrow range of 1.2–2.5 mM $CoHex^{3+}$ was observed. The columnar hexagonal phase persisted in the 2.5–30 mM $CoHex^{3+}$ range. The long-range order of the NCP columnar phase disappeared or was reduced by acetylation of the H4 tails, acidic patch neutralization.

Single tail deletion effects result in diversity of the spectra. The H4 tail deletion results in spectra similar to those of WT-NCP for both Mg^{2+} and $CoHex^{3+}$, with the formation of columnar hexagonal phases. Deletion of gH2A tails in the presence of Mg^{2+} or $CoHex^{3+}$ produces spectra with multiple peaks, indicating highly ordered structures with peak positions that are not in agreement with the previously reported columnar hexagonal phase (9). Deletion of H2B and H3 tails results in the NCP columnar phase in the presence of Mg^{2+}. In the presence of $CoHex^{3+}$, multiple peaks at high q (>0.15 $Å^{-1}$) indicate ordering in the gH2B spectrum, but the low intensity of q_1 with the high-intensity q_2 peak with a shoulder and the absence of regular NCP stacking peak make phase identification difficult. The gH3 spectrum in the presence of $CoHex^{3+}$ is similar to that of gH2A. The electrostatic contribution of the tail deletion effect may be due to the fact that NCP columns lacking H2B and H3 tails are more electronegative than columns lacking H2A and H4 tails that form columnar hexagonal phases. Recent coarse-grained simulations from our laboratory, using an advanced coarse-grained NCP model that reproduces the detailed shape of the NCP core and geometry and the flexibility of the tails, confirmed that in phases of aggregated NCPs, the H2A and H4 tails stabilize the NCP-NCP stacking contact, whereas the H3 and H2B tails are responsible for screening and bridging interactions between the lateral surfaces of the contacting NCPs (17). The gH2A and gH3 samples are special cases because an unknown structure is observed. The tail deletion also changes the shape of the NCPs with a different and probably more dynamic DNA wrapping around the HO, besides changing the charge and charge distribution, thereby allowing the formation of new contacts. One particular effect of the tail removal is the unpeeling of the DNA ends, which makes the NCP resemble the chromatosome, a complex of NCP with the linker histone H1 (77).

In the case of four samples with more than one tail removed (namely, gH3gH4, gH2AgH3gH4, gH2AgH2BgH3, and gNCP), the aggregates produced featureless spectra, indicating the formation of an isotropic NCP phase with no long-range order in the presence of Mg^{2+} or $CoHex^{3+}$. We conclude that the removal of the H3 tail in combination with any other tail is sufficient to prevent the formation of NCP columns, possibly by inhibiting NCP stacking. The H3 tail is the largest of the four tails, and its essential role in long-range NCP order is not surprising.

Our observation that the effects of the absence of H2A and H2B tails resulted in novel (to our knowledge), highly ordered structures in the NCP aggregates is intriguing. These effects may be biologically relevant, because H2A/H2B dimers are more dynamic than $(H3/H4)_2$ tetramers, and the H2A histone family has the largest number of variants. The highly ordered phases observed in this work deserve to be characterized using high-resolution methods such as cryo-EM and crystallography. The role of individual tails may be addressed by NMR. In addition, studies of aggregates of NCP reconstituted with $(H3/H4)_2$ tetramers only or with H2A histone variants may contribute to our understanding of the role of histone tails.

Finally, it must be strongly emphasized that the reconstitution of tailless constructs results in NCPs with different particle shapes, which likely is caused by a different, more dynamic DNA wrapping around the HO with unwrapping at the DNA ends, resulting in a more dynamic, heterogeneous system. For this reason, the effects observed for the tailless systems could be due both to the change in NCP particle structure and to the absence of the tails, which is expected to result in decreased inter-NCP interactions and diminished order. Therefore, the above conclusions and discussions regarding tailless systems should be considered tentative, and further characterization of these systems is warranted.

SUPPORTING MATERIAL

Supporting Materials and Methods, Supporting Results, three tables, and 22 figures are available at http://www.biophysj.org/biophysj/supplemental/S0006-3495(16)30067-4.

AUTHOR CONTRIBUTIONS

N.K. and L.N. designed research. N.V.B., Y.L., C.-J.S., and N.K. performed research. A.A., C.-F.L., and R.Y. contributed analytical tools. N.V.B., Y.L., and N.K. analyzed data. N.V.B., N.K., and L.N. wrote the manuscript.

ACKNOWLEDGMENTS

We thank Dr. Curt Davey and Prof. Timothy Richmond for gifts of the plasmids encoding DNA and core histones, and Prof. Martin Zacharias for

sharing coordinates of the NCPs obtained in molecular dynamics simulations.

This work was supported by the Singapore Agency for Science Technology and Research (A*STAR) through the Biomedical Research Council (grant 10/1/22/19/666) and by the Singapore Ministry of Education Academic Research Fund (AcRF) through a Tier 3 grant (MOE2012-T3-1-001).

REFERENCES

1. Luger, K., A. W. Mäder, …, T. J. Richmond. 1997. Crystal structure of the nucleosome core particle at 2.8 A resolution. *Nature.* 389:251–260.
2. Davey, C. A., D. F. Sargent, …, T. J. Richmond. 2002. Solvent mediated interactions in the structure of the nucleosome core particle at 1.9 a resolution. *J. Mol. Biol.* 319:1097–1113.
3. Woodcock, C. L., A. I. Skoultchi, and Y. Fan. 2006. Role of linker histone in chromatin structure and function: H1 stoichiometry and nucleosome repeat length. *Chromosome Res.* 14:17–25.
4. Hansen, J. C. 2002. Conformational dynamics of the chromatin fiber in solution: determinants, mechanisms, and functions. *Annu. Rev. Biophys. Biomol. Struct.* 31:361–392.
5. Raspaud, E., I. Chaperon, …, F. Livolant. 1999. Spermine-induced aggregation of DNA, nucleosome, and chromatin. *Biophys. J.* 77:1547–1555.
6. de Frutos, M., E. Raspaud, …, F. Livolant. 2001. Aggregation of nucleosomes by divalent cations. *Biophys. J.* 81:1127–1132.
7. Mangenot, S., A. Leforestier, …, F. Livolant. 2002. Salt-induced conformation and interaction changes of nucleosome core particles. *Biophys. J.* 82:345–356.
8. Mangenot, S., E. Raspaud, …, F. Livolant. 2002. Interactions between isolated nucleosome core particles. A tail bridging effect? *Eur. Phys. J. E.* 7:221–231.
9. Mangenot, S., A. Leforestier, …, F. Livolant. 2003. X-ray diffraction characterization of the dense phases formed by nucleosome core particles. *Biophys. J.* 84:2570–2584.
10. Mangenot, S., A. Leforestier, …, F. Livolant. 2003. Phase diagram of nucleosome core particles. *J. Mol. Biol.* 333:907–916.
11. Bertin, A., A. Leforestier, …, F. Livolant. 2004. Role of histone tails in the conformation and interactions of nucleosome core particles. *Biochemistry.* 43:4773–4780.
12. Bertin, A., M. Renouard, …, D. Durand. 2007. H3 and H4 histone tails play a central role in the interactions of recombinant NCPs. *Biophys. J.* 92:2633–2645.
13. Bertin, A., S. Mangenot, …, F. Livolant. 2007. Structure and phase diagram of nucleosome core particles aggregated by multivalent cations. *Biophys. J.* 93:3652–3663.
14. Bertin, A., D. Durand, …, S. Mangenot. 2007. H2A and H2B tails are essential to properly reconstitute nucleosome core particles. *Eur. Biophys. J.* 36:1083–1094.
15. Korolev, N., A. Allahverdi, …, L. Nordenskiöld. 2012. The polyelectrolyte properties of chromatin. *Soft Matter.* 8:9322–9333.
16. Luger, K., and T. J. Richmond. 1998. The histone tails of the nucleosome. *Curr. Opin. Genet. Dev.* 8:140–146.
17. Fan, Y., N. Korolev, …, L. Nordenskiöld. 2013. An advanced coarse-grained nucleosome core particle model for computer simulations of nucleosome-nucleosome interactions under varying ionic conditions. *PLoS One.* 8:e54228.
18. Woodcock, C. L., and S. Dimitrov. 2001. Higher-order structure of chromatin and chromosomes. *Curr. Opin. Genet. Dev.* 11:130–135.
19. Wolffe, A. P., and J. J. Hayes. 1999. Chromatin disruption and modification. *Nucleic Acids Res.* 27:711–720.
20. Liu, Y., C. Lu, …, L. Nordenskiöld. 2011. Influence of histone tails and H4 tail acetylations on nucleosome-nucleosome interactions. *J. Mol. Biol.* 414:749–764.
21. Lewis, P. N., J. G. Guillemette, and S. Chan. 1988. Histone accessibility determined by lysine-specific acetylation in chicken erythrocyte nuclei. *Eur. J. Biochem.* 172:135–145.
22. Perry, M., and R. Chalkley. 1981. The effect of histone hyperacetylation on the nuclease sensitivity and the solubility of chromatin. *J. Biol. Chem.* 256:3313–3318.
23. Perry, M., and R. Chalkley. 1982. Histone acetylation increases the solubility of chromatin and occurs sequentially over most of the chromatin. A novel model for the biological role of histone acetylation. *J. Biol. Chem.* 257:7336–7347.
24. Tse, C., T. Sera, …, J. C. Hansen. 1998. Disruption of higher-order folding by core histone acetylation dramatically enhances transcription of nucleosomal arrays by RNA polymerase III. *Mol. Cell. Biol.* 18:4629–4638.
25. Horn, P. J., and C. L. Peterson. 2002. Molecular biology. Chromatin higher order folding—wrapping up transcription. *Science.* 297:1824–1827.
26. Wolffe, A. P. 1998. Chromatin: Structure and Function. Academic Press, San Diego, CA.
27. Turner, B. M. 1991. Histone acetylation and control of gene expression. *J. Cell Sci.* 99:13–20.
28. Calestagne-Morelli, A., and J. Ausió. 2006. Long-range histone acetylation: biological significance, structural implications, and mechanisms. *Biochem. Cell Biol.* 84:518–527.
29. Kurdistani, S. K., S. Tavazoie, and M. Grunstein. 2004. Mapping global histone acetylation patterns to gene expression. *Cell.* 117:721–733.
30. Szerlong, H. J., J. E. Prenni, …, J. C. Hansen. 2010. Activator-dependent p300 acetylation of chromatin in vitro: enhancement of transcription by disruption of repressive nucleosome-nucleosome interactions. *J. Biol. Chem.* 285:31954–31964.
31. Korolev, N., N. V. Berezhnoy, …, L. Nordenskiöld. 2012. A universal description for the experimental behavior of salt-(in)dependent oligocation-induced DNA condensation. *Nucleic Acids Res.* 40:2808–2821.
32. Bloomfield, V. A. 1997. DNA condensation by multivalent cations. *Biopolymers.* 44:269–282.
33. Finch, J. T., L. C. Lutter, …, A. Klug. 1977. Structure of nucleosome core particles of chromatin. *Nature.* 269:29–36.
34. Finch, J. T., R. S. Brown, …, A. Klug. 1981. X-ray diffraction study of a new crystal form of the nucleosome core showing higher resolution. *J. Mol. Biol.* 145:757–769.
35. Vasudevan, D., E. Y. Chua, and C. A. Davey. 2010. Crystal structures of nucleosome core particles containing the '601' strong positioning sequence. *J. Mol. Biol.* 403:1–10.
36. Leforestier, A., J. Dubochet, and F. Livolant. 2001. Bilayers of nucleosome core particles. *Biophys. J.* 81:2414–2421.
37. Leforestier, A., and F. Livolant. 1997. Liquid crystalline ordering of nucleosome core particles under macromolecular crowding conditions: evidence for a discotic columnar hexagonal phase. *Biophys. J.* 73:1771–1776.
38. Schalch, T., S. Duda, …, T. J. Richmond. 2005. X-ray structure of a tetranucleosome and its implications for the chromatin fibre. *Nature.* 436:138–141.
39. Dorigo, B., T. Schalch, …, T. J. Richmond. 2004. Nucleosome arrays reveal the two-start organization of the chromatin fiber. *Science.* 306:1571–1573.
40. Robinson, P. J. J., L. Fairall, …, D. Rhodes. 2006. EM measurements define the dimensions of the "30-nm" chromatin fiber: evidence for a compact, interdigitated structure. *Proc. Natl. Acad. Sci. USA.* 103:6506–6511.
41. Song, F., P. Chen, …, G. Li. 2014. Cryo-EM study of the chromatin fiber reveals a double helix twisted by tetranucleosomal units. *Science.* 344:376–380.
42. Scheffer, M. P., M. Eltsov, …, A. S. Frangakis. 2012. Nucleosomes stacked with aligned dyad axes are found in native compact chromatin in vitro. *J. Struct. Biol.* 178:207–214.

43. Castro-Hartmann, P., M. Milla, and J.-R. Daban. 2010. Irregular orientation of nucleosomes in the well-defined chromatin plates of metaphase chromosomes. *Biochemistry.* 49:4043–4050.

44. Livolant, F., S. Mangenot, …, D. Durand. 2007. Are liquid crystalline properties of nucleosomes involved in chromosome structure and dynamics? *Philos. Trans. A Math. Phys. Eng. Sci.* 364:2615–2633.

45. Garcés, R., R. Podgornik, and V. Lorman. 2015. Antipolar and anticlinic mesophase order in chromatin induced by nucleosome polarity and chirality correlations. *Phys. Rev. Lett.* 114:238102.

46. Manna, F. A., V. L. Lorman, …, B. Žekš. 2007. Polarity and chirality in NCP mesophases and chromatin fibers. *Mol. Cryst. Liq. Cryst.* 478:83–97.

47. Lorman, V., R. Podgornik, and B. Žekš. 2005. Correlated and decorrelated positional and orientational order in the nucleosomal core particle mesophases. *Europhys. Lett.* 69:1017–1023.

48. Howell, S. C., K. Andresen, …, X. Qiu. 2013. Elucidating internucleosome interactions and the roles of histone tails. *Biophys. J.* 105:194–199.

49. Luger, K., T. J. Rechsteiner, and T. J. Richmond. 1999. Preparation of nucleosome core particle from recombinant histones. *Methods Enzymol.* 304:3–19.

50. Wang, X., C. He, …, J. Ausio. 2001. Effects of histone acetylation on the solubility and folding of the chromatin fiber. *J. Biol. Chem.* 276:12764–12768.

51. Shogren-Knaak, M., H. Ishii, …, C. L. Peterson. 2006. Histone H4-K16 acetylation controls chromatin structure and protein interactions. *Science.* 311:844–847.

52. Kan, P.-Y., X. Lu, …, J. J. Hayes. 2007. The H3 tail domain participates in multiple interactions during folding and self-association of nucleosome arrays. *Mol. Cell. Biol.* 27:2084–2091.

53. Wang, X., and J. J. Hayes. 2007. Site-specific binding affinities within the H2B tail domain indicate specific effects of lysine acetylation. *J. Biol. Chem.* 282:32867–32876.

54. Routh, A., S. Sandin, and D. Rhodes. 2008. Nucleosome repeat length and linker histone stoichiometry determine chromatin fiber structure. *Proc. Natl. Acad. Sci. USA.* 105:8872–8877.

55. Robinson, P. J. J., W. An, …, D. Rhodes. 2008. 30 nm chromatin fibre decompaction requires both H4-K16 acetylation and linker histone eviction. *J. Mol. Biol.* 381:816–825.

56. Wang, X., and J. J. Hayes. 2008. Acetylation mimics within individual core histone tail domains indicate distinct roles in regulating the stability of higher-order chromatin structure. *Mol. Cell. Biol.* 28:227–236.

57. Korolev, N., A. Allahverdi, …, L. Nordenskiöld. 2010. Electrostatic origin of salt-induced nucleosome array compaction. *Biophys. J.* 99:1896–1905.

58. Allahverdi, A., R. Yang, …, L. Nordenskiöld. 2011. The effects of histone H4 tail acetylations on cation-induced chromatin folding and self-association. *Nucleic Acids Res.* 39:1680–1691.

59. Zhou, B. R., H. Feng, …, Y. Bai. 2012. Histone H4 K16Q mutation, an acetylation mimic, causes structural disorder of its N-terminal basic patch in the nucleosome. *J. Mol. Biol.* 421:30–37.

60. Pollard, K. J., M. L. Samuels, …, C. L. Peterson. 1999. Functional interaction between GCN5 and polyamines: a new role for core histone acetylation. *EMBO J.* 18:5622–5633.

61. Dorigo, B., T. Schalch, …, T. J. Richmond. 2003. Chromatin fiber folding: requirement for the histone H4 N-terminal tail. *J. Mol. Biol.* 327:85–96.

62. McBryant, S. J., J. Klonoski, …, J. C. Hansen. 2009. Determinants of histone H4 N-terminal domain function during nucleosomal array oligomerization: roles of amino acid sequence, domain length, and charge density. *J. Biol. Chem.* 284:16716–16722.

63. Kalashnikova, A. A., M. E. Porter-Goff, …, J. C. Hansen. 2013. The role of the nucleosome acidic patch in modulating higher order chromatin structure. *J. R. Soc. Interface.* 10:20121022.

64. Lowary, P. T., and J. Widom. 1998. New DNA sequence rules for high affinity binding to histone octamer and sequence-directed nucleosome positioning. *J. Mol. Biol.* 276:19–42.

65. Luger, K., T. J. Rechsteiner, and T. J. Richmond. 1999. Expression and purification of recombinant histones and nucleosome reconstitution. *Methods Mol. Biol.* 119:1–16.

66. Dyer, P. N., R. S. Edayathumangalam, …, K. Luger. 2004. Reconstitution of nucleosome core particles from recombinant histones and DNA. *Methods Enzymol.* 375:23–44.

67. Jeng, U.-S., C. H. Su, …, K. S. Liang. 2010. A small/wide-angle X-ray scattering instrument for structural characterization of air–liquid interfaces, thin films and bulk specimens. *J. Appl. Cryst.* 43:110–121.

68. Safinya, C. R. 2001. Structures of lipid-DNA complexes: supramolecular assembly and gene delivery. *Curr. Opin. Struct. Biol.* 11:440–448.

69. Roccatano, D., A. Barthel, and M. Zacharias. 2007. Structural flexibility of the nucleosome core particle at atomic resolution studied by molecular dynamics simulation. *Biopolymers.* 85:407–421.

70. Korolev, N., O. V. Vorontsova, and L. Nordenskiöld. 2007. Physicochemical analysis of electrostatic foundation for DNA-protein interactions in chromatin transformations. *Prog. Biophys. Mol. Biol.* 95:23–49.

71. Svergun, D. I., C. Barberato, and M. H. J. Koch. 1995. CRYSOL—a program to evaluate X-ray solution scattering of biological macromolecules from atomic coordinates. *J. Appl. Cryst.* 28:768–773.

72. Schneidman-Duhovny, D., M. Hammel, and A. Sali. 2010. FoXS: a web server for rapid computation and fitting of SAXS profiles. *Nucleic Acids Res.* 38:W540–W544.

73. Zhou, J., J. Y. Fan, …, D. J. Tremethick. 2007. The nucleosome surface regulates chromatin compaction and couples it with transcriptional repression. *Nat. Struct. Mol. Biol.* 14:1070–1076.

74. Leforestier, A., S. Fudaley, and F. Livolant. 1999. Spermidine-induced aggregation of nucleosome core particles: evidence for multiple liquid crystalline phases. *J. Mol. Biol.* 290:481–494.

75. Matulis, D., I. Rouzina, and V. A. Bloomfield. 2000. Thermodynamics of DNA binding and condensation: isothermal titration calorimetry and electrostatic mechanism. *J. Mol. Biol.* 296:1053–1063.

76. Korolev, N., Y. Zhao, …, L. Nordenskiöld. 2012. The effect of salt on oligocation-induced chromatin condensation. *Biochem. Biophys. Res. Commun.* 418:205–210.

77. Zhou, B. R., J. Jiang, …, Y. Bai. 2015. Structural mechanisms of nucleosome recognition by linker histones. *Mol. Cell.* 59:628–638.

Biophysical Journal, Volume *110*

Supplemental Information

The Influence of Ionic Environment and Histone Tails on Columnar Order of Nucleosome Core Particles

Nikolay V. Berezhnoy, Ying Liu, Abdollah Allahverdi, Renliang Yang, Chun-Jen Su, Chuan-Fa Liu, Nikolay Korolev, and Lars Nordenskiöld

Biophysical Journal

Supporting Material

The Influence of Ionic Environment and Histone Tails on Columnar Order of Nucleosome Core Particles

Nikolay V. Berezhnoy,[1] Ying Liu,[1] Abdollah Allahverdi,[1] Renliang Yang,[1] Chun-Jen Su,[2] Chuan-Fa Liu,[1] Nikolay Korolev,[1] and Lars Nordenskiöld[1,*]

[1]School of Biological Sciences, Nanyang Technological University, Singapore; and [2]National Synchrotron Radiation Research Center, Hsinchu, Taiwan

*Correspondence: larsnor@ntu.edu.sg

Supporting Materials and Methods

Preparation and purification of histones

Genes coding wild-type and modified *X. laevis* core histones H2A, H2B, H3 and H4 in the pET-3a plasmids were expressed using *E. coli* strain BL21 (DE3) pLysS. Gene constructs of mutated histones H4-K16Q, H4-QuadQ and H2A-STT were prepared from wild type genes using QuickChange site-directed mutagenesis kit (1). Gene constructs of tailless histones gH2A, gH2B, gH3 and gH4 were cloned from wild type genes using PCR (2, 3). Gene construct with H4 residues 20-102 and Lys20Cys mutation used in preparation of H4-K16Ac and H4-QuadAc was prepared from wild type gene using PCR (1).

Single colonies of *E. coli* transformed with histone constructs were grown in 2xTY medium containing appropriate antibiotics, the histone expression was induced by 0.4 mM isopropyl-β,D-thiogalactopyranoside (IPTG) at OD_{600} = 0.6. After 3 hours of incubation at 37˚C (WT) or 30˚C (modified histones) bacterial cells were harvested by centrifugation (7,000 g, 7 min, 25°C). The bacteria resuspended in 100 mL of wash buffer (1 M Tris·HCl, 100 mM NaCl and 1 mM β-mercaptoethanol) were lysed by flash freezing in liquid nitrogen and thawing. The cell suspension was sonicated until the loss of viscosity using SONICS Vibra-Cell ultrasonic processor at amplitude of 25% with two-second-pulse. The inclusion bodies containing histones were precipitated from the sonication mixture (12,000 g, 15 min, 4°C), and washed three times in 200 mL of wash buffer containing 1% (v/v) Triton X-100 by repeated resuspension and centrifugation, followed by washing twice with 200 mL wash buffer to remove the detergent. The histones from inclusion bodies were dissolved in 1 mL of dimethylsulfoxide (DMSO) at room temperature, followed by addition of 40 mL of S-200 unfolding buffer (7 M guanidinium·HCl, 20 mM Na-acetate at pH 5.2 and 10 mM dithiothreitol (DTT)).

The histones were purified at room temperature by gel-filtration and cation-exchange chromatography and the purity was checked by 18% SDS-PAGE. The histones were purified using HiPrep 26/60 Sephacryl S-200 HR gel-filtration column (GE Healthcare Life Sciences) in SAUDE-1000 buffer (7 M deionized urea, 20 mM Na-acetate at pH 5.2, 1000 mM NaCl, 5 mM β-mercaptoethanol and 1 mM EDTA). Purified histones were dialyzed against water containing 5 mM β-mercaptoethanol, using Spectra/Por dialysis tubing (MWCO 3,500 Da), centrifuged to remove aggregates (10,000 rpm, 10 min at 4 ˚C) and lyophilized.

The wild type histones were dissolved in SAUDE-200 buffer (7 M deionized urea, 20 mM Na-acetate at pH 5.2, 200 mM NaCl, 5 mM β-mercaptoethanol and 1 mM EDTA) and the modified histones were dissolved in SAUDE-0 buffer (7 M deionized urea, 20 mM Na-acetate at pH 5.2, 5 mM β-mercaptoethanol and 1 mM EDTA) and purified in a 15% - 40% gradient of SAUDE-1000 buffer using Resource S 6 mL cation exchange column (GE Healthcare Life Sciences).

Acetylated forms of the histone H4, H4K16Ac and H4-QuadAc (tetraacetylated form at the positions 5, 8, 12 and 16) were obtained by native chemical ligation (NCL) and S-alkylation reactions as described in earlier work (1, 4). Briefly NCL reaction was carried with 1CL reaction was cathioester and truncated histone H4(20-102)K20C in ligation buffer (6M GdnHCl, 0.2M phosphate, 20 mM TCEP, 1.5% benzyl mercaptan, pH 8.0). The ligation product was purified by semi-preparative HPLC. Next, the S-alkylation reaction was performed between the ligation product and 2-bromoethylamine dissolved in alkylation buffer (4M GdnHCl, 1M HEPES, 10mM D/L-methionine, 5mM TCEP, pH 7.8). The product was isolated either with C4 semi-preparative

HPLC or by dialysis against 2-mercaptoethanol-containing water. It was shown (4) that S-alkylated analog of lysine at position 20 of the histone H4 does not influence of biophysical and biochemical properties of the nucleosome arrays constructed with this form the of the H4 histone.

Histone octamer refolding and purification

Lyophilized core histone proteins H2A, H2B, H3 and H4 (WT or modified) were dissolved in HO-unfolding buffer (7 M guanidinium HCl, 10 mM Tris·HCl, pH 7.5 and 10 mM DDT). The concentration of each nucleosome histone or the mutants was determined by the absorbance at λ = 276 nm, with the molar extinction coefficients calculated from the amino acid composition (5). The histones were combined at molar ratio of H2A:H2B:H3:H4 = 1:1:1.2:1.2 and a final protein concentration of 1 mg/mL. The dialysis against HO-refolding buffer (2 M NaCl, 10 mM Tris·HCl at pH7.5, 1 mM EDTA and 5 mM beta-mercaptoethanol) was carried at room temperature using Spectra/Por dialysis membrane (MWCO 6-8 kDa). The HO solution was centrifuged (9,000 g, 10 min, 20°C), concentrated to 10 mg/mL using Amicon ultra centrifugal filter (MWCO 10 kDa) and purified using the HiPrep 26/60 Sephacryl S-200 HR gel filtration column in the HO-refolding buffer. The purity and completeness of the HO refolding was checked by 18% SDS-PAGE. The octamer solutions were stored in 50% glycerol at –20°C.

DNA preparation

The DNA used in this work to reconstitute nucleosome core particle was the 145 bp '601' Widom nucleosome-positioning sequence (6). In a few SAXS measurements, NCP reconstituted with the 147 bp palindromic human α-satellite DNA fragment (7, 8) was used.

The pUC19 plasmid containing eight copies of 145 bp '601' DNA flanked by EcoRV restriction enzyme recognition sites was a gift from the laboratory of Dr. Curt. A. Davey (Nanyang Technological University).

The pUC19 plasmid containing 145 bp DNA was amplified in *E. coli* HB101 and extracted by alkaline lysis method. The plasmid was purified by treated with RNase, phenol, and precipitated by PEG 6000. The plasmid was digested by EcoRV, and the 145 bp DNA was separated from the vector by PEG 6000 and extracted by chloroform: 3-methyl-1-butanol mixture (v/v = 24:1). The purity of 145 bp DNA was checked by 10% PAGE.

NCP reconstitution

The 145 bp DNA and HO were mixed in a range of molar ratios in a total volume of 200 µl, containing 6 µM (0.544 mg/mL) 145 bp DNA, 4-6 µM HO, 2 M KCl and 10 mM DTT. The mixture in a Spectra/Por dialysis membrane (MWCO 6-8 kDa) was dialyzed in buffer (20 mM Tris HCl pH 7.5, 1mM EDTA and 1mM DTT) with step-wise decrease of KCl concentration: 1.3 M, 0.85 M, 0.65 M, 0.45 M and 10 mM. The purity of NCP and the absence of free 145 bp DNA was checked on 5% PAGE. The optimal ratio was chosen for the large-scale preparation. The yield was comparable for all NCP types, wild type, mutated and with deleted tails. The presence of less than 5% of free DNA was tolerated in the NCP preparations used for precipitation by cations and solution measurements. The free DNA remained in the solution during NCP precipitation by Mg^{2+}. The presence of free DNA did not affect the scattering in H2A-STT sample, the scattering was comparable with WT-NCP and H4-K16Q.

Small angle X-ray scattering (SAXS)

The NCP aggregates at 8 mg/mL of the final NCP concentration in 20 mM Tris-HCl buffer (pH 7.5) were prepared by adding 40 μl of multivalent cation salt solution into 160 μL of 10 mg/mL NCP stock solution. The suspended NCP aggregates were transferred into the quartz capillary d = 1.5 - 2 mm (Charles Supper Company, USA), sealed with wax and centrifuged to precipitate aggregates.

Measurements were made with X-ray flux of 14.0 keV (λ= 0.886 Å) at the Beamline 23A SWAXS endstation of the National Synchrotron Radiation Research Center (Hsinchu, Taiwan) (9). The X-ray beam was directed at the center of the precipitate above the curved bottom of the capillary. Scattering profiles were recorded with charge-coupled device-based area detector (MarCCD165, Mar Evanston, IL, USA) at 1.75 m sample-to-detector distance. The scattering wave vector $q = 4\pi \cdot sin(\theta)/\lambda$ (2θ is the scattering angle) was calibrated with silver behenate. The two-dimensional diffraction pattern was circularly averaged into one-dimensional q versus I spectrum. The raw Bragg reflection data were corrected for background scattering and sample transmission before analyzed with the software OriginPro 9.

Table S1. Composition of the NCP samples studied by SAXS.

	NCP type	NCP concentration, mg/mL	Cation	Cation concentration, mM
1	WT-NCP	1.25 – 17	K^+	10 – 100
		8	Mg^{2+}	3 – 80
		8	$CoHex^{3+}$	1.2 – 30
		8	Spd^{3+}	3.88 – 11.64
		8	Spm^{4+}	1.45 – 5.82
2	H4-K16Q	8	Mg^{2+}	12 – 50
		8	$CoHex^{3+}$	0.8 – 5
3	H4-K16Ac	8	Mg^{2+}	5 – 50
		8	$CoHex^{3+}$	1.7 – 8
4	H4-QuadQ	8	Mg^{2+}	10 – 70
		8	$CoHex^{3+}$	0.8 – 3.7
5	H4-QuadAc	8	Mg^{2+}	10, 25
		8	$CoHex^{3+}$	4, 5
6	H2A-STT	8	Mg^{2+}	4 – 28
		8	$CoHex^{3+}$	1.2 – 4
7	gH2A	8	Mg^{2+}	15 – 30
		8	$CoHex^{3+}$	1.5 – 3
8	gH2B	8	Mg^{2+}	10 – 30
		8	$CoHex^{3+}$	1.5 – 5
9	gH3	8	Mg^{2+}	15 – 30
		8	$CoHex^{3+}$	1.5, 2

10	gH4	8	Mg^{2+}	15 – 30
		8	$CoHex^{3+}$	1.5 – 3
11	gH2AgH2B	8	Mg^{2+}	10 – 30
		8	$CoHex^{3+}$	1.5 – 10
12	gH3gH4	8	Mg^{2+}	10 – 30
		8	$CoHex^{3+}$	1.5 – 5
13	gH2AgH3gH4	8	Mg^{2+}	10 – 30
		8	$CoHex^{3+}$	1.5 – 5
14	gH2AgH2BgH3	8	Mg^{2+}	10 – 30
		8	$CoHex^{3+}$	1.5 – 5
15	gNCP	8	Mg^{2+}	12 – 100
		8	$CoHex^{3+}$	1.5 – 27

Abbreviations: **WT**, wild type; H4-K16Q, NCP with K→Q mutation at Lys16 of the H4 histone; **H4-K16Ac**, NCP with acetylated Lys16 of the H4 histone; **H4-QuadQ**, NCP with K→Q mutations at positions Lys5, Lys8, Lys12, Lys16 of the H4 histone; **H4-QuadAc**, NCP with acetylated Lys5, Lys8, Lys12, Lys16 of the H4 histone; **H2A-STT**, NCP with mutations D90S+E91T+E92T in the H2A histone (these 3 mutations significantly reduced negative charge of the acidic patch on the surface of histone octamer which is important for nucleosome-nucleosome interactions) ; **gH2A**, histone octamer with globular **H2A** histone (a.a. at positions 1-12 and 119-129 were truncated); **gH2B**, histone octamer with tailless H2B histone (a.a. at positions 1-21 were truncated); **gH3**, a.a. at positions 1-26) of the H3 histone were removed; **gH4**, a.a. at positions 1-19) of the H4 histone were removed; **gH2AgH2B**, NCP with tailless H2A and H2B histones; **gH3gH4**, NCP with tailless H3 and H4 histones; **gH2AgH3gH4**, NCP with tailless H2A, H3 and H4 histones; **gH2AhH2BgH3**, NCP with tailless H2A, H2B and H3 histones; **gNCP**, NCP with all four histones being tailless

Supporting Results

Collection of SAXS spectra

Figures S1 – S22 present SAXS spectra measured for all types of NCP at various concentrations of cations with most of the data obtained for the NCP samples aggregated by addition of Mg^{2+} and $CoHex^{3+}$.

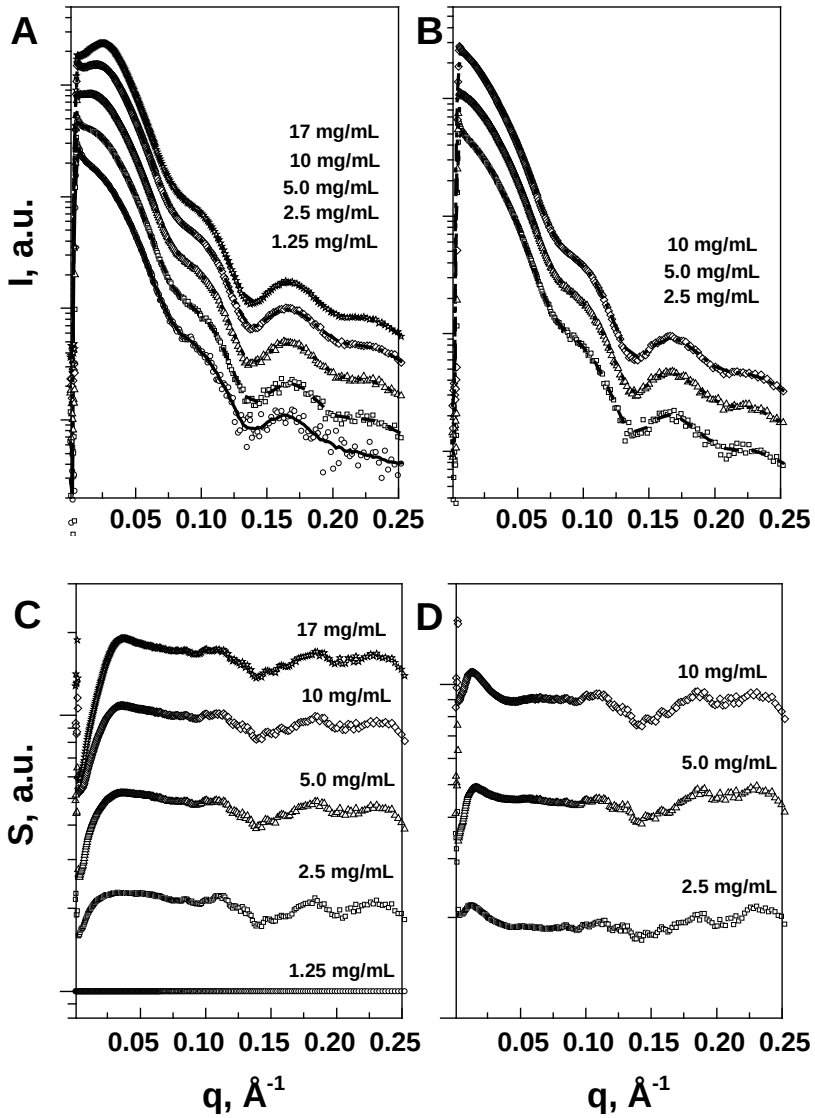

FIGURE S1. SAXS spectra (**A,B**) and calculated structure factors, S, (**C,D**) of the solutions of wild type (WT) NCP in 10 mM (**A,C**) and 100 mM (**B,D**) KCl. Concentration of the NCP in solution varied from 1.25 to 17 mg/mL (**A,C**) and from 2.5 to 10 mg/mL (**B,D**) (from bottom to top, indicated in the graphs). In **A** and **B** points are experimental data lines are 10-point averaged smoothing. Structure factors (C,D) were calculated by dividing corresponding SAXS spectra by spectrum obtained for 1.25 mg/mL solution of NCP in 10 mM KCl (i.e. under the conditions of weak and repulsive NCP-NCP interaction).

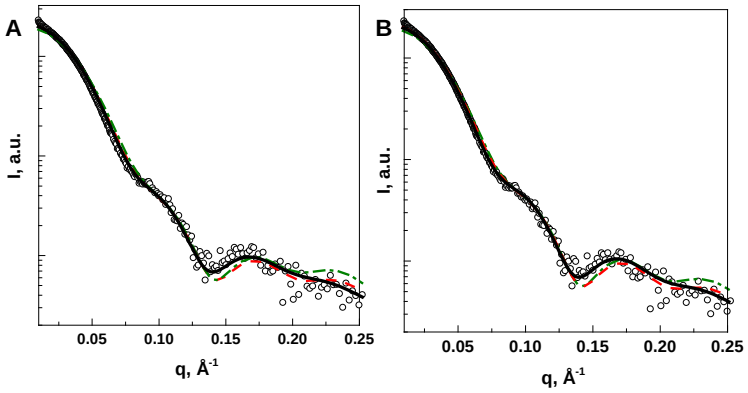

FIGURE S2. Comparison of the experimental and calculated SAXS spectra of the WT-NCP. Experimental data is for 145 bp '601' WT-NCP solution (1.25 mg/mL, 10 mM KCl). Theoretical curves were calculated using (**A**) CRYSOL software (10) or (**B**) FoXS web server (11) from three variants of the 1KX5 NCP crystal structure (8). In (**A**) and (**B**) points are experimental data; lines are results of calculations using different variants of the 1KX5 structure: (black solid line) coordinates according to the MD simulations of isolated NCP (12) with tails collapsed on the DNA and globular histone core; (red dashed line) structure as in the NCP crystal; (green dot-dashed line) tail coordinates were removed from the pdb file

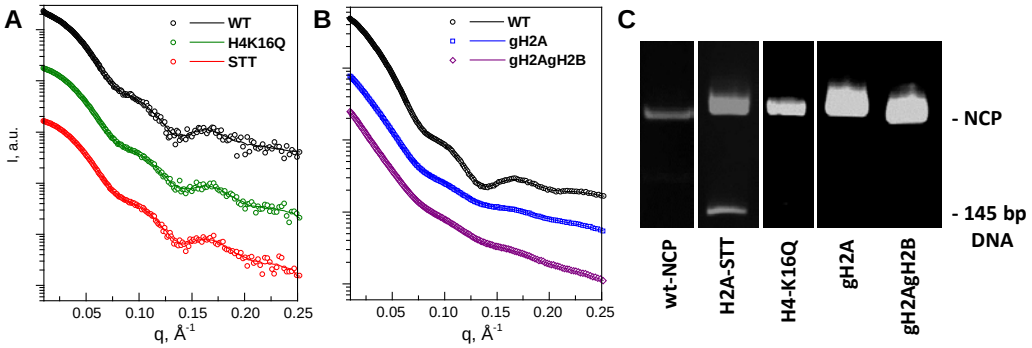

FIGURE S3. (**A**) and (**B**). Comparison of the SAXS solution spectra obtained (**A**) for WT, H4-K16Q and H2A-STT NCPs at 1.25 mg/mL concentration of NCP in 10 mM KCl; for (**B**) WT, gH2A and gH2AgH2B at 10 mg/mL concentration of NCP in 100 mM KCl. Points are experimental readings, curves are 10-point smoothing of the data. (**C**). 5% PAGE analysis of the NCP reconstitutions. Type of the NCP indicated in the figure.

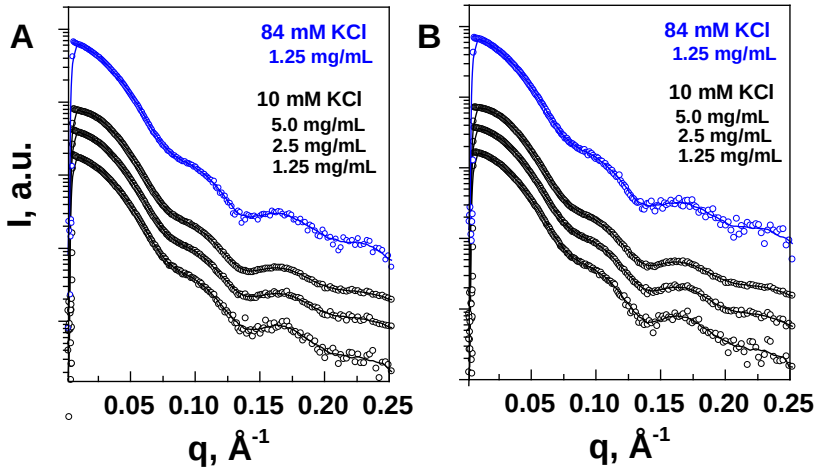

FIGURE S4. SAXS spectra of the solutions of H4-K16Q (**A**) and H2A-STT (**B**) NCPs. Concentration of the NCP in 84 mM KCl was equal to 1.25 mg/mL (blue points and curves) or was varied from 1.25 to 5 mg/mL in 10 mM KCl (black points and curves) (indicated in the graphs). Points are experimental data lines are 10 point averaged smoothing.

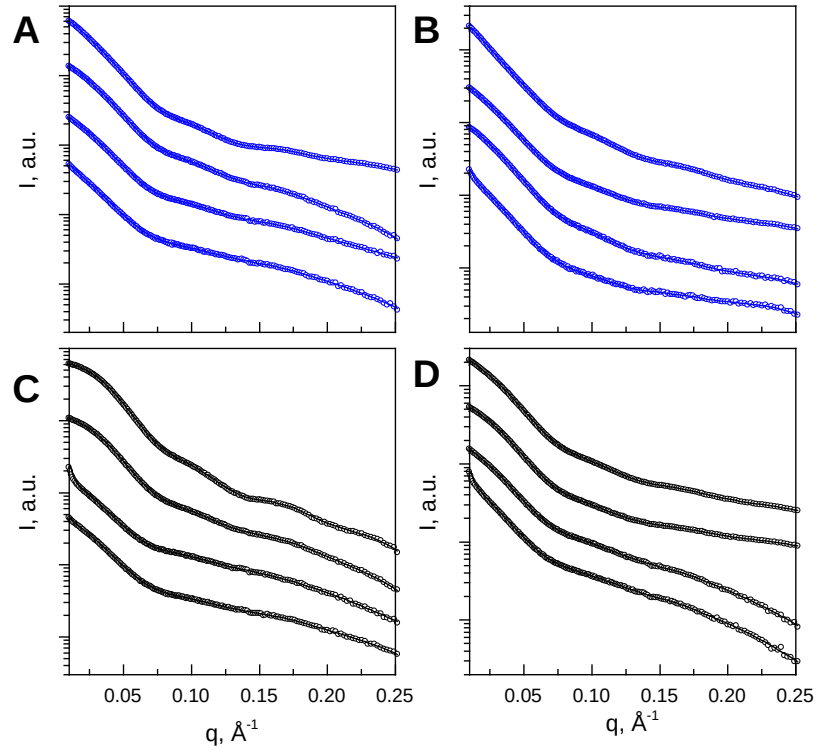

FIGURE S5. SAXS spectra of the solutions of gH2A (**A,C**) and gH2AgH2B (**B,D**) NCPs recorded in (A, B) 100 mM (blue points and curves) and (C, D) 10 mM KCl (black points and curves). In all graphs, NCP concentrations are equal 1.25, 2.5, 5.0 and 10.0 mg/mL and increase from bottom to top. Points are experimental data lines are 10 point averaged smoothing.

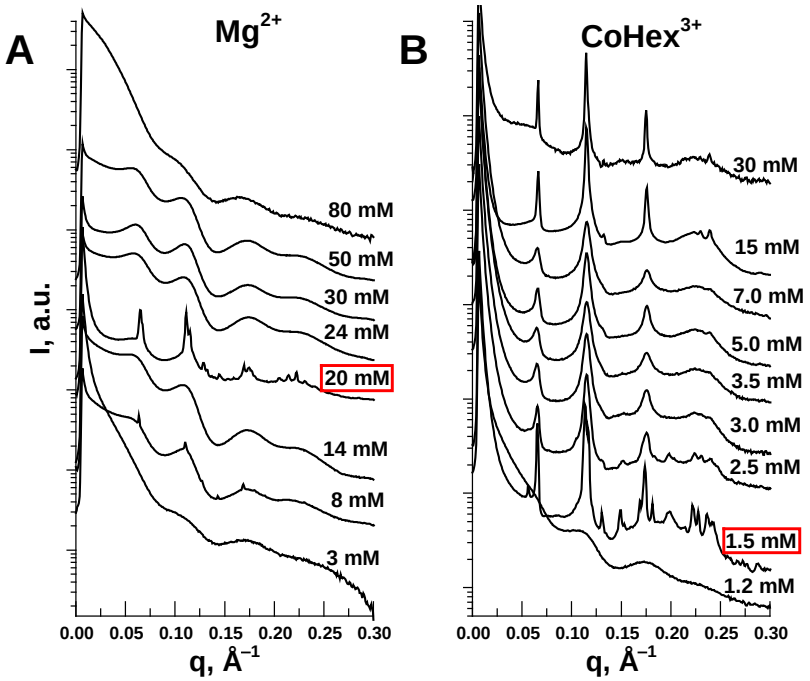

FIGURE S6. SAXS spectra of the wild type (WT) NCP in the presence of various concentrations of Mg^{2+} (**A**) and cobalt(III)hexammine^{3+} ($CoHex^{3+}$; **B**). Cation concentrations are indicated on the graphs with concentration of the most organized NCP phase highlighted by red box.

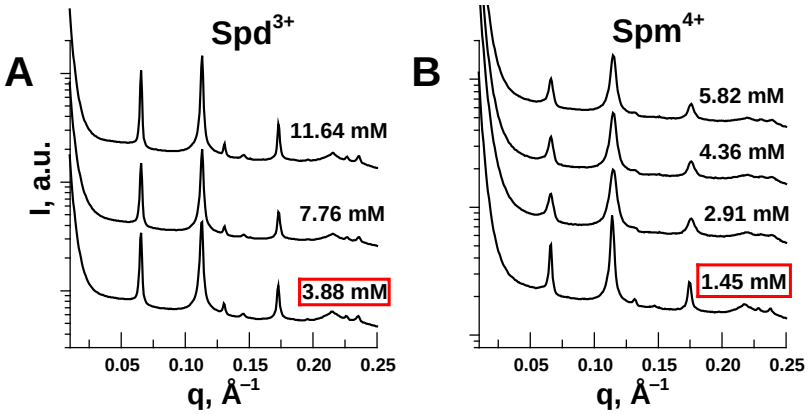

FIGURE S7. SAXS spectra the wild type (WT) NCP in the presence of various concentrations of spermidine^{3+} (Spd^{3+}; **A**) and spermine^{4+} (Spm^{4+}; **B**). Cation concentrations are indicated on the graphs with concentration of the most organized NCP phase highlighted by red box.

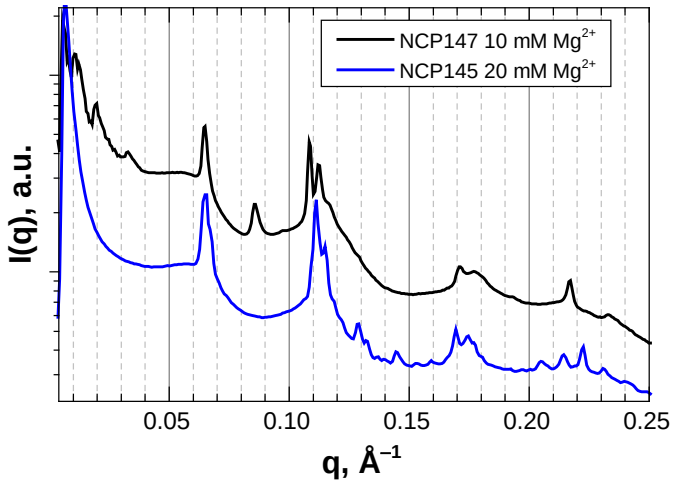

FIGURE S8. Comparison of the SAXS spectra of the two NCP samples aggregated by Mg^{2+} with different DNA templates. NCP147 (black line, top spectrum) was reconstituted on 147 bp α-satellite human DNA sequence (13); NCP145 (blue line, bottom spectrum) was prepared from the 145 bp Widom high affinity '601' DNA (6).

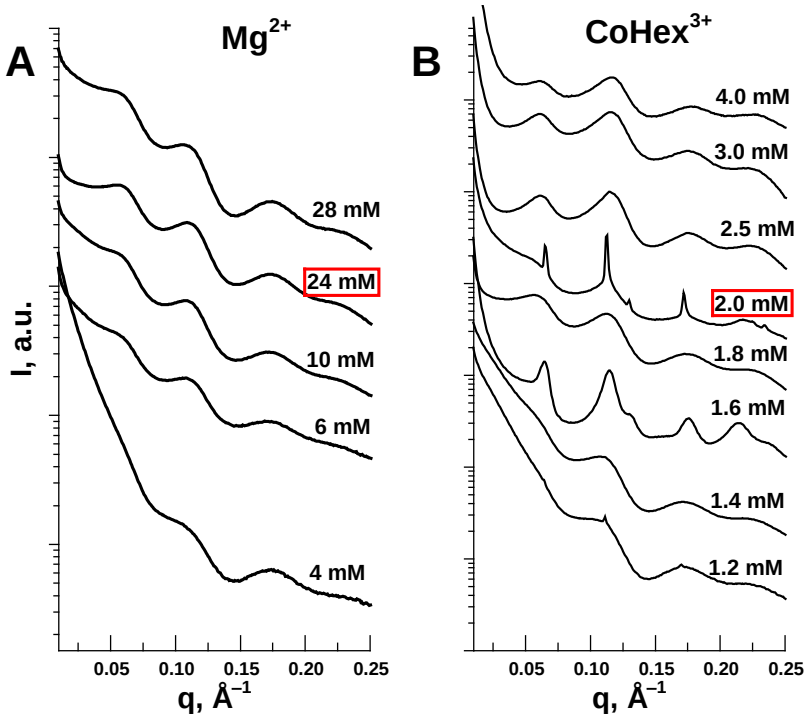

FIGURE S9. SAXS spectra of the NCP containing STT mutation of the H2A histone (D90S+E91T+E92T) in the presence of various concentrations of Mg^{2+} (**A**) and $CoHex^{3+}$ (**B**). Cation concentrations are indicated on the graphs with concentration of the most organized NCP phase highlighted by red box.

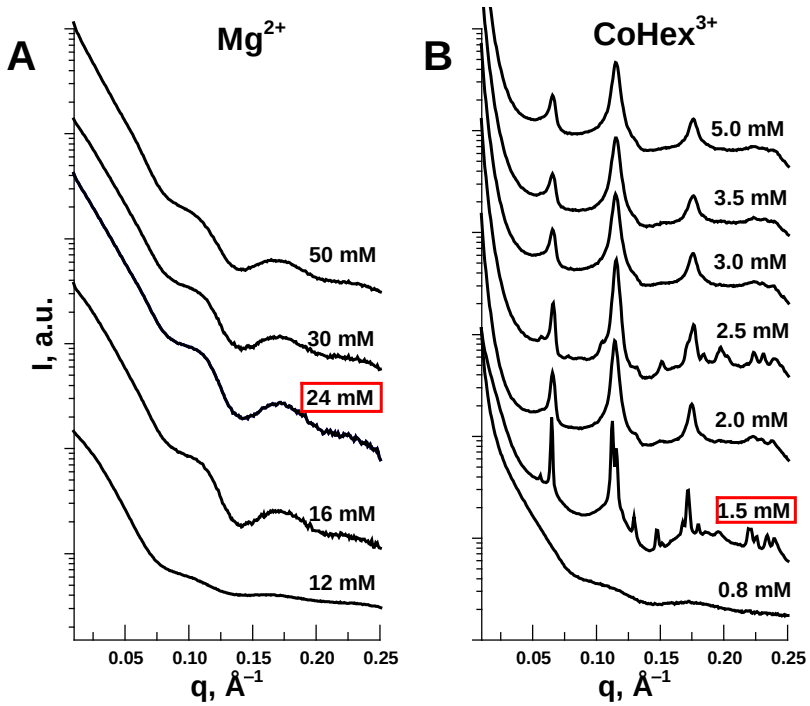

FIGURE S10. SAXS spectra of the NCP containing K16Q mutation of the H4 histone (H4-K16Q) in the presence of various concentrations of Mg^{2+} (**A**) and $CoHex^{3+}$ (**B**). Cation concentrations are indicated on the graphs with concentration of the most organized NCP phase highlighted by red box.

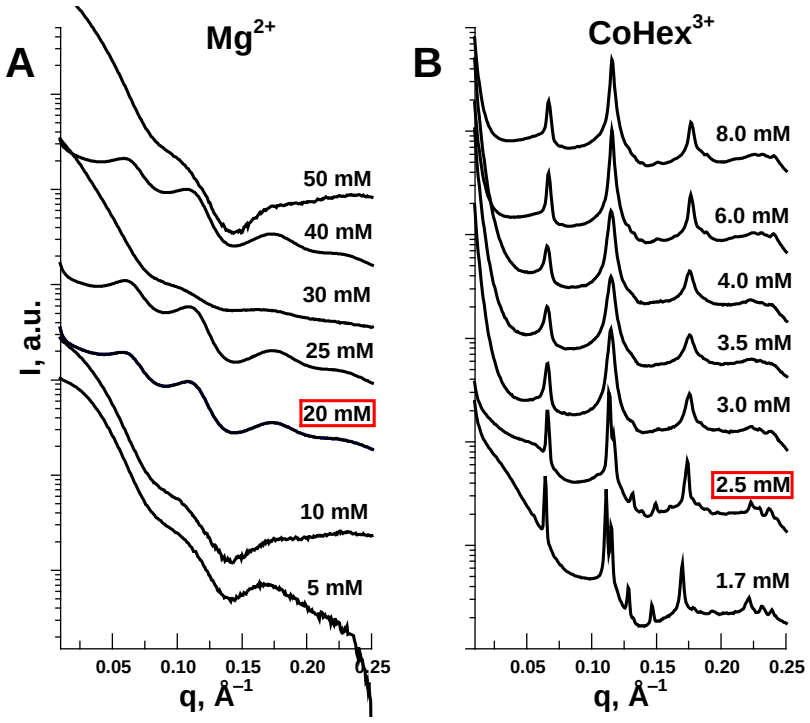

FIGURE S11. SAXS spectra of the NCP containing acetylated Lys16 in the H4 histone (H4-K16Ac) in the presence of various concentrations of Mg^{2+} (**A**) and $CoHex^{3+}$ (**B**). Cation concentrations are indicated on the graphs with concentration of the most organized NCP phase highlighted by red box.

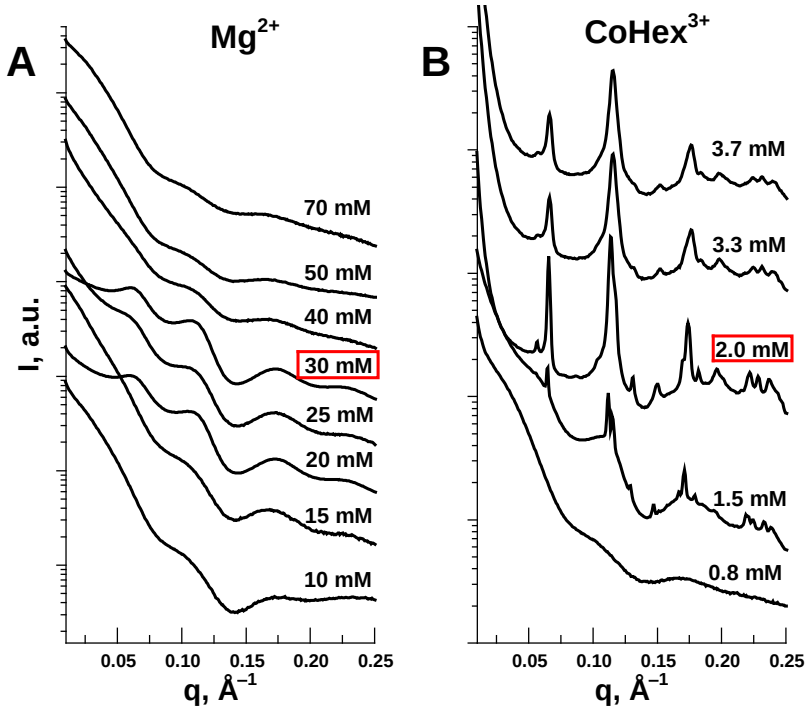

FIGURE S12. SAXS spectra of the NCP containing K5Q, K8Q, K12Q, K16Q mutations of the H4 histone (H4-QuadQ) in the presence of various concentrations of Mg^{2+} (**A**) and $CoHex^{3+}$ (**B**). Cation concentrations are indicated on the graphs with concentration of the most organized NCP phase highlighted by red box.

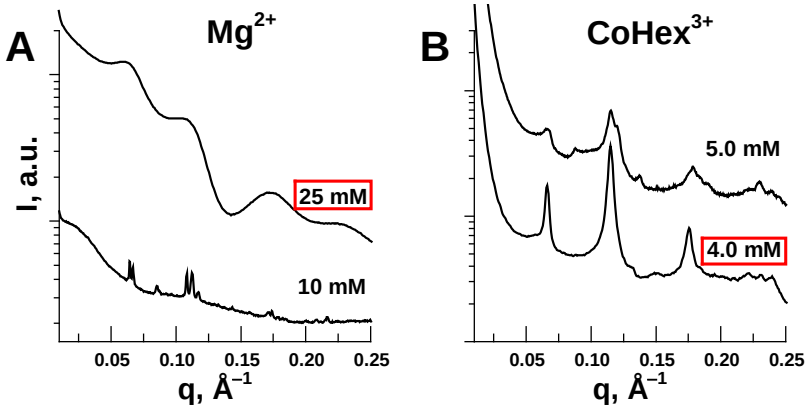

FIGURE S13. SAXS spectra of the NCP containing acetylated Lys5, Lys8, Lys12, Lys16 in the H4 histone (H4-QuadAc) in the presence of various concentrations of Mg^{2+} (**A**) and $CoHex^{3+}$ (**B**). Cation concentrations are indicated on the graphs with concentration of the most organized NCP phase highlighted by red box. Spectra at 10 mM Mg^{2+} and 5 mM $CoHex^{3+}$ were obtained with NCP containing 147 bp α-satellite human DNA sequence.

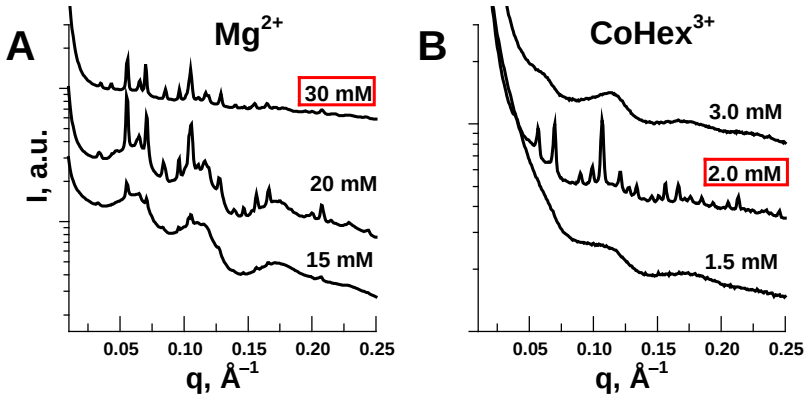

FIGURE S14. SAXS spectra of the NCP containing tailless histone H2A (gH2A) in the presence of various concentrations of Mg^{2+} (**A**) and $CoHex^{3+}$ (**B**). Cation concentrations are indicated on the graphs with concentration of the most organized NCP phase highlighted by red box.

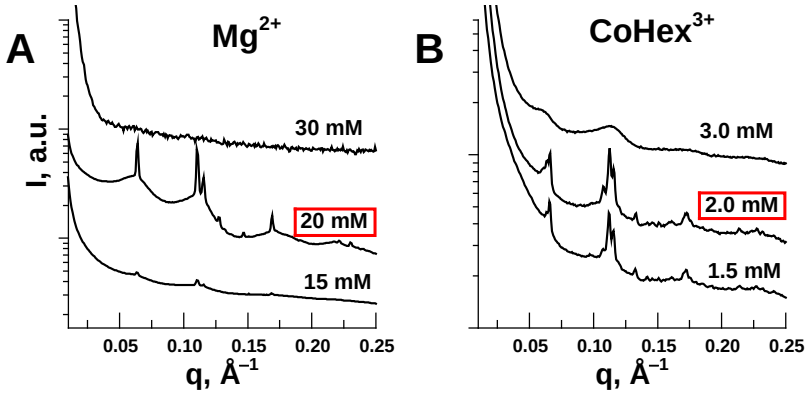

FIGURE S15. SAXS spectra of the NCP containing tailless histone H4 (gH4) in the presence of various concentrations of Mg^{2+} (**A**) and $CoHex^{3+}$ (**B**). Cation concentrations are indicated on the graphs with concentration of the most organized NCP phase highlighted by red box.

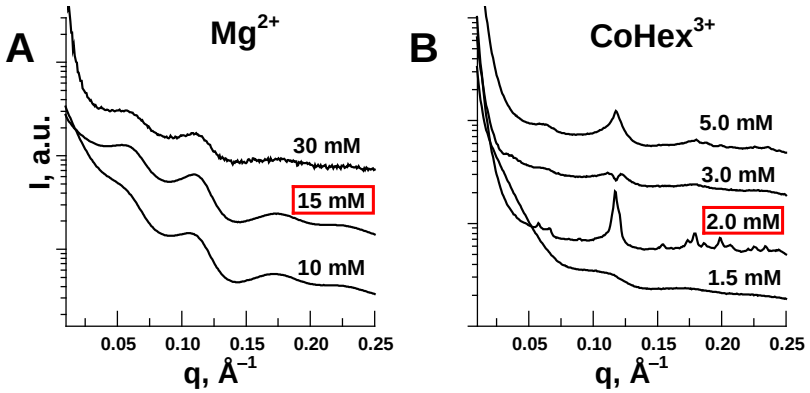

FIGURE S16. SAXS spectra (**A,B**) and calculated structure factors (**C,D**) of the NCP containing tailless histone H2B (gH2B) in the presence of various concentrations of Mg^{2+} (**A,C**) and $CoHex^{3+}$ (**B,D**). Cation concentrations are indicated on the graphs with concentration of the most organized NCP phase highlighted by red box.

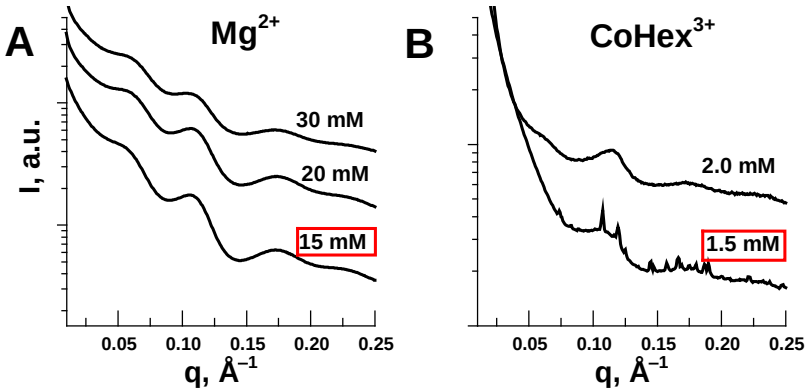

FIGURE S17. SAXS spectra of the NCP containing tailless histone H3 (gH3) in the presence of various concentrations of Mg^{2+} (A) and $CoHex^{3+}$ (**B**). Cation concentrations are indicated on the graphs with concentration of the most organized NCP phase highlighted by red box.

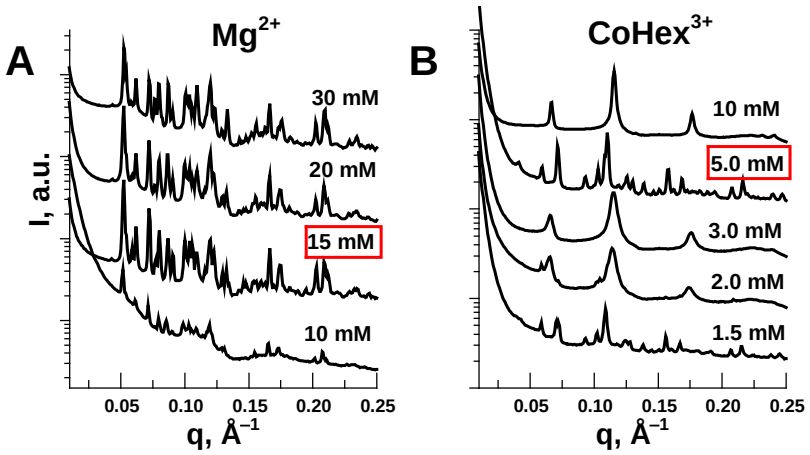

FIGURE S18. SAXS spectra of the NCP containing tailless histones H2A and H2B (gH2AgH2B) in the presence of various concentrations of Mg^{2+} (**A**) and $CoHex^{3+}$ (**B**). Cation concentrations are indicated on the graphs with concentration of the most organized NCP phase highlighted by red box.

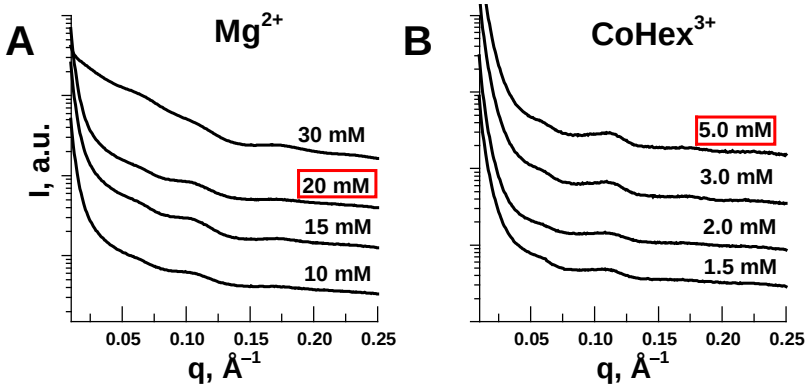

FIGURE S19. SAXS spectra of the NCP containing tailless histones H3 and H4 (gH3gH4) in the presence of various concentrations of Mg^{2+} (**A**) and $CoHex^{3+}$ (**B**). Cation concentrations are indicated on the graphs with concentration of the most organized NCP phase highlighted by red box.

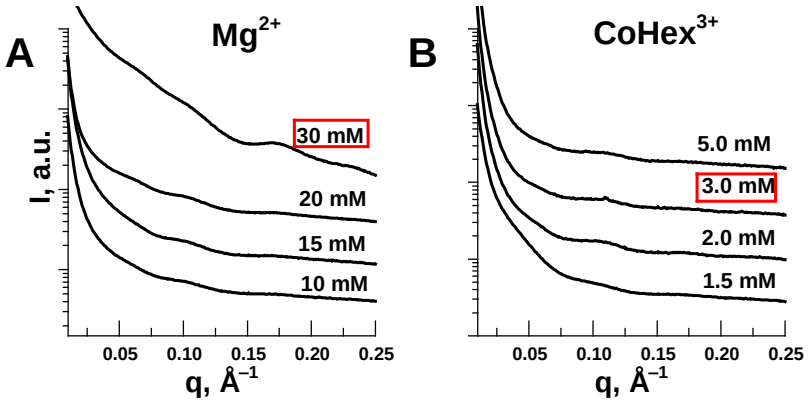

FIGURE S20. SAXS spectra of the NCP containing tailless histones H2A, H3 and H4 (gH2AgH3gH4) in the presence of various concentrations of Mg^{2+} (**A**) and $CoHex^{3+}$ (**B**). Cation concentrations are indicated on the graphs with concentration of the most organized NCP phase highlighted by red box.

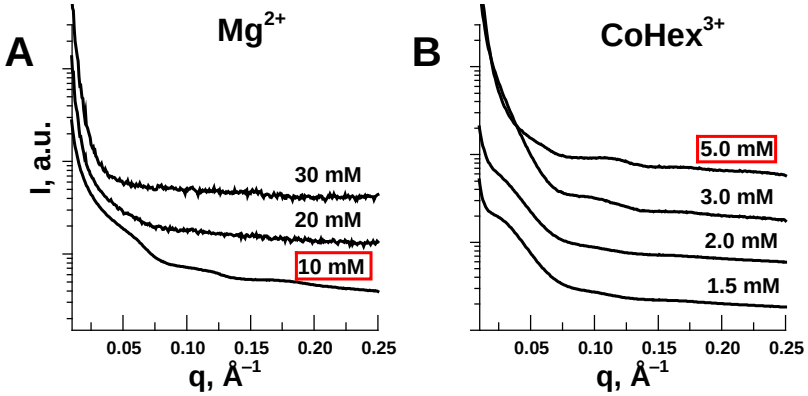

FIGURE S21. SAXS spectra of the NCP containing tailless histones H2A, H2B and H3 (gH2AgH2BgH3) in the presence of various concentrations of Mg^{2+} (**A**) and $CoHex^{3+}$ (**B**). Cation concentrations are indicated on the graphs with concentration of the most organized NCP phase highlighted by red box.

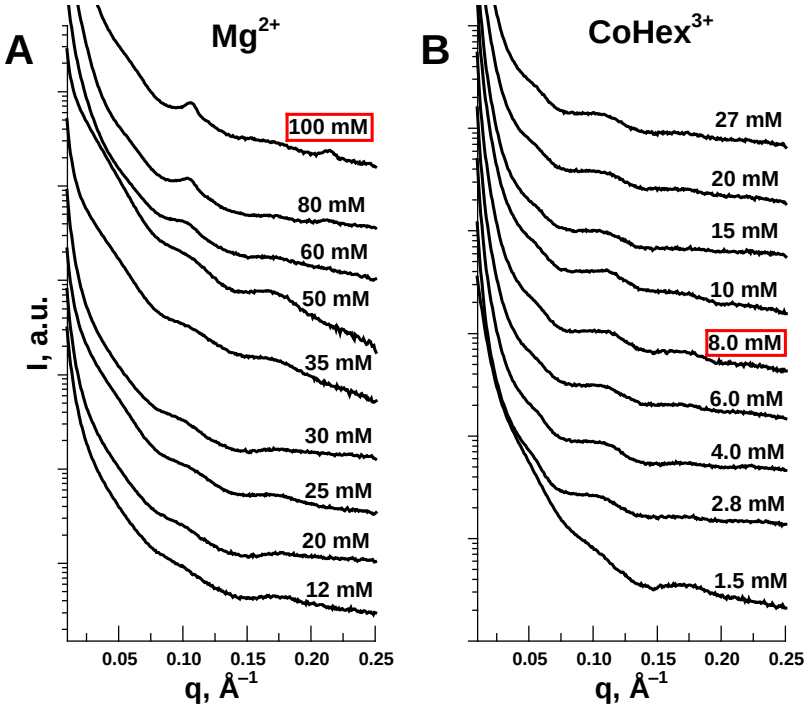

FIGURE S22. SAXS spectra of the NCP containing tailless histones (gNCP) in the presence of various concentrations of Mg^{2+} (**A**) and $CoHex^{3+}$ (**B**). Cation concentrations are indicated in the graphs with concentration of the most organized NCP phase highlighted by red box.

Table S2. Characteristic peak positions and the derived structure parameters a_H and h. SAXS spectra of the gH2A and gH2AgH2B samples are not included since for these samples structure of ordered phase is not known that prevents reliable interpretation of the peaks.

Sample	Cation	Concen-tration, mM	q_1	$q_2=\sqrt{3}\,q_1$	$q_3=\sqrt{4}\,q_1$	$q_4=\sqrt{7}\,q_1$	q_{1h}	$q_{2h}=2\,q_{1h}$	a_H (Å)	h (Å)	Phase
WT-NCP	Mg^{2+}	20 mM	0.065	0.115	0.128	0.170	0.111	0.222	111.6	56.5	3D orthorhombic
	$CoHex^{3+}$	1.5 mM	0.065	0.117	0.13	0.174	0.114	0.228	110.9	55.3	3D orthorhombic
	Spd^{3+}	3.88 mM	0.065	0.113	0.131	0.173	0.113	0.226	111.5	55.7	2D hexagonal
	Spm^{4+}	1.45 mM	0.066	0.114	0.132	0.174	0.114	0.228	110.3	55.1	2D hexagonal
H4K16Q	Mg^{2+}	24 mM									NCP isotropic
	$CoHex^{3+}$	1.5 mM	0.065	0.116	0.13	0.172	0.112	0.225	111.8	55.9	3D orthorhombic
H4K16Ac	Mg^{2+}	20 mM									NCP columnar
	$CoHex^{3+}$	2.5 mM	0.066	0.117	0.131	0.174	0.114	0.227	110.1	55.4	3D orthorhombic
H4-QuadQ	Mg^{2+}	30 mM									NCP columnar
	$CoHex^{3+}$	2.0 mM	0.066	0.117	0.131	0.174	0.114	0.228	110.7	55.2	3D orthorhombic
H4-QuadAc	Mg^{2+}	25 mM									NCP columnar
	$CoHex^{3+}$	4 mM	0.066	-*	0.132	0.175	0.115	0.231	109.9	54.6	2D hexagonal
H2A-STT	Mg^{2+}	24 mM									NCP columnar
	$CoHex^{3+}$	2.0 mM	0.065	-*	0.130	0.172	0.112	0.224	111.1	55.9	2D hexagonal
gH4	Mg^{2+}	20 mM	0.064	0.115	0.127	0.169	0.111	0.22	113.9	56.8	2D hexagonal
	$CoHex^{3+}$	2.0 mM	0.066	0.116	0.133	0.172	0.112	0.224	109.9	55.9	3D orthorhombic

gH2B	Mg^{2+}	15 mM									NCP columnar
	$CoHex^{3+}$	2.0 mM	0.066	0.117	-	0.173			110.8		3D orthorhombic
gH3	Mg^{2+}	15 mM									NCP columnar
	$CoHex^{3+}$	1.5 mM									unknown
gH3gH4	Mg^{2+}	20 mM									NCP isotropic
	$CoHex^{3+}$	5.0 mM									NCP isotropic
gH2AgH3gH4	Mg^{2+}	30 mM									NCP isotropic
	$CoHex^{3+}$	3.0 mM					0.11			57.1	NCP isotropic
gH2AgH2BgH3	Mg^{2+}	10 mM									NCP isotropic
	$CoHex^{3+}$	5.0 mM									NCP isotropic
g-NCP	Mg^{2+}	100 mM					0.106	0.214		59.4	NCP isotropic
	$CoHex^{3+}$	8.0 mM									NCP isotropic

*The first order NCP stacking peak is merged with the second order hexagonal-phase peak, and the accurate peak position cannot be determined;

- Data not available

Table S3. The domain size was estimated from the full width at half maximum (fwhm) of the first diffraction peaks in columnar hexagonal phases for the most ordered samples from Fig. 4 of the main text.

Sample	Cation	q_1					q_{1h}				
		Position	fwhm	a_H, Å	$s(a_H)$, nm	Columns	Position	fwhm	h, Å	s(h), nm	Stacked NCP
WT-NCP	Mg^{2+}	0.0650	0.0027	111.62	232	21	0.111	0.0022	56.52	280	50
WT-NCP	$CoHex^{3+}$	0.0654	0.0018	110.94	349	31	0.114	0.0028	55.31	224	41
WT-NCP,	Spd^{3+}	0.0651	0.0016	111.45	383	34	0.113	0.0023	55.65	273	49
WT-NCP	Spm^{4+}	0.0658	0.0020	110.29	313	28	0.114	0.0027	55.12	237	43
H4-K16Ac	$CoHex^{3+}$	0.0659	0.0019	110.09	338	31	0.114	0.0019	55.36	338	61
H4-K16Q	$CoHex^{3+}$	0.0649	0.0013	111.79	476	43	0.112	0.0019	55.90	324	58
H4-QuadAc	$CoHex^{3+}$	0.0660	0.0038	109.93	164	15	0.115	0.0044	54.64	142	26
H4-QuadQ	$CoHex^{3+}$	0.0656	0.0018	110.67	345	31	0.114	0.0029	55.21	217	39
H2A-STT	$CoHex^{3+}$	0.0653	0.0023	111.11	269	24	0.112	0.0020	55.90	322	58
gH4	Mg^{2+}	0.0637	0.0011	113.90	556	49	0.111	0.0014	56.81	462	81
gH4	$CoHex^{3+}$	0.0660	0.0018	109.93	355	32	0.112	0.0025	55.90	255	46
gH2B	$CoHex^{3+}$	0.0655	0.0050	110.77	126	11	-	-	-	-	-

- Data not available

REFERENCES

1. Allahverdi, A., R. Yang, N. Korolev, Y. Fan, C. A. Davey, C. F. Liu, and L. Nordenskiöld. 2011. The effects of histone H4 tail acetylations on cation-induced chromatin folding and self-association. Nucleic Acids Res. 39:1680–1691
2. Dorigo, B., T. Schalch, K. Bystricky, and T. J. Richmond. 2003. Chromatin fiber folding: requirement for the histone H4 N-terminal tail. J.Mol.Biol. 327:85-96.
3. Liu, Y., C. Lu, Y. Yang, Y. Fan, R. Yang, C.-F. Liu, N. Korolev, and L. Nordenskiöld. 2011. Influence of histone tails and H4 tail acetylations on nucleosome–nucleosome interactions. J.Mol.Biol. 414:749–764.
4. Li, F., A. Allahverdi, R. Yang, B. Lua G, X. Zhang, Y. Cao, N. Korolev, L. Nordenskiöld, and C. F. Liu. 2011. A direct method for site-specific protein acetylation. Angew.Chem.Int.Ed. 50:9611 –9614.
5. Gill, S. C., and P. H. von Hippel. 1989. Calculation of protein extinction coefficients from amino acid sequence data. Anal.Biochem. 182:319-326.
6. Lowary, P. T., and J. Widom. 1998. New DNA sequence rules for high affinity binding to histone octamer and sequence-directed nucleosome positioning. J.Mol.Biol. 276:19-42.
7. Luger, K., A. W. Mader, R. K. Richmond, D. F. Sargent, and T. J. Richmond. 1997. Crystal structure of the nucleosome core particle at 2.8 Å resolution. Nature 389:251-260.
8. Davey, C. A., D. F. Sargent, K. Luger, A. W. Maeder, and T. J. Richmond. 2002. Solvent mediated interactions in the structure of nucleosome core particle at 1.9 Å resolution. J.Mol.Biol. 319:1097-1113.
9. Jeng, U.-S., C. H. Su, C.-J. Su, K.-F. Liao, W.-T. Chuang, Y.-H. Lai, J.-W. Chang, Y.-J. Chen, Y.-S. Huang, M.-T. Lee, K.-L. Yu, J.-M. Lin, D.-G. Liu, C.-F. Chang, C.-Y. Liu, C.-H. Changa, and K. S. Liang. 2010. A small/wide-angle X-ray scattering instrument for structural characterization of air–liquid interfaces, thin films and bulk specimens. J.Appl.Cryst. 43:110-121.
10. Svergun, D. I., C. Barberato, and M. H. J. Koch. 1995. CRYSOL - a program to evaluate X-ray solution scattering of biological macromolecules from atomic coordinates. J. Appl. Cryst. 28:768-773.
11. Schneidman-Duhovny, D., M. Hammel, and A. Sali. 2010. FoXS: a web server for rapid computation and fitting of SAXS profiles. Nucleic Acids Res. 38:W540-W544.
12. Roccatano, D., A. Barthel, and M. Zacharias. 2007. Structural flexibility of the nucleosome core particle at atomic resolution studied by molecular dynamics simulation. Biopolymers 85:407-421.
13. Luger, K., T. J. Rechsteiner, and T. J. Richmond. 1999. Preparation of nucleosome core particle from recombinant histones. Methods Enzymol. 304:3-19.